COLLEGE of SCIENCE
UtahStateUniversity

GEOSCIENCES

September 8, 2020

Solid Earth

Dear Dr. Eichhubl,

We are pleased to submit for your consideration our revised manuscript "Spatiotemporal history of fault-fluid interaction in the Hurricane fault, western U.S." by Jace M. Koger and Dennis L. Newell. The two reviews were very constructive, and both recommended minor revisions. We have incorporated all of the major suggested changes. Below we provide a detailed response to each comment and how we have changed the manuscript text and figures. We feel that the revised manuscript is much stronger, and we truly appreciate the time the reviewers spent evaluating our work.

In addition to the revised manuscript and supplemental, we have included with this document, pdf's of the track-changes versions of the main text and supplemental.

Thank you for considering our work for publication in *Solid Earth*!

Best regards,

Dennis Newell

Corresponding Author

4505 Old Main Hill
Logan, UT 84322-4505
P-435-797-1273
F-435-797-1588
geo@usu.edu

GEO SCIENCES

In the following we detail how we have addressed each of the comments and suggestions from Billy Andrews and Matthew Steele-MacInnis. In addition, some edits were made to the manuscript pdf file by Billy Andrews, and these have been incorporated into the revised manuscript.

Comments and suggestions from Billy Andrews

Major comments

MC1: Lack of structural data and the field context of the samples.

A large omission from the manuscript is structural data from the different field sites and the structural relationship of the described features. This makes it difficult to place the geochemical analysis into a field setting. Wide-angle field photographs, and the inclusion of some of the field photographs in the supplementary information would greatly aid in this. I was surprised no fault or vein data was presented, either in the supplementary information or as a stereographic projection associated with the geological history of the fault. Your geochemical analysis is fantastic, but you quickly lose context without linking this to the observed structural relationships. You highlight, and I strongly agree, that the structural diagenesis, and in particular field relations and timing of these events is fundamental to the geochemical analysis. It is clear from your supplementary information, methodology section, and in part the results that this has been considered during fieldwork, However, when reading the manuscript I was often left to read between the lines, or search out images in the supplementary information, to work out what this looks like. Please consider further elaborating on the structural relationships and moving some field photographs from the supplementary information into the main text so the reader has context to the geochemical analysis.

Author Response:

We agree that the omission of details associated with the structural data detracts from the interpretation of the geochemical results. To rectify this, the following changes have been made.

1) A new supplemental figure (map) has been added that includes stereonets from all the field sites. The stereonet data is color-coded to show the different vein sets and measured fractures. In total these stereonets include 477 orientation measurements.

MC2: Confusing age relationships & unclear fracture attributes (Section 4.1).

I found the vein and fracture data presented in section 4.1 rather confusing, something that was not aided by the already highlighted points in MC1. You make reference to fracture density on line 257, however, I found it very unclear how you calculated this and whether it referred to P_{10} that is most often referred to as fracture intensity (f/m), or P_{20} that is more often referred to as fracture density. If this data was collected using scanline methods, what was the length/radius/area of the scanlines as this can have a very large impact on the reported values. If not how was the reported 'densities' calculated? This will be compounded by the fact you appear to have several fracture corridors, as suggested in line 226 where P_{10} will locally drastically increase.

Author Response:

We measured the fracture intensity (f/m) and incorrectly called this fracture density. The text is changed to make this clear. Also, we used a linear scanline method, using a tape measure oriented approximately orthogonal to the main fault trace. For the footwall outcrops observed along the Hurricane fault, this worked well as most observed fractures are intersected this way. We recognize that there can be bias using this simple method, but for the field sites visited this was the most efficient method. The length of the scanlines was variable and based on the available exposures. Drainages and canyons that cut the fault and run approximately orthogonal to the fault were the focus of the data collection due to the best exposures. Some canyons are relatively long (> 1 km), allowing the transect to traverse the damage zone completely. Other small drainages only penetrate part of the damage zone. Yes, as you point out there are some fracture corridors in the damage zone that have greater fracture intensity. We have updated the text to make it clear how the data was collected. Specifically, details of the methods were added to section 3.1, and section 4.1 and the supplement were updated with the correct terminology.

Regarding the reported 'orientation sets' I have some the following specific questions:

1, How do the orientation sets relate to the age sets? i.e. are there systematic cross cutting relationships or are both orientations reactivated throughout the 4 stages derived from the geochemistry?

Author Response:

In a very general sense, there seems to be systematic cross-cutting relationships along the fault. However, we downplay this in the paper given the limited geochronological data set. Locally, where we have U-Th data, the cross-cutting relationships hold up (e.g., Fig 5). Using the geochemistry and geochronology, to a first order it appears that veins associated with the lower salinity fluids with a strong meteoric water affinity are older (including the 280 – 540 ka veins), compared to the saltier fluids characterized in the 86 – 113 ka veins (Fig. S7). In order to really flesh this out and present a more comprehensive paragenetic history linked to vein set, significantly more geochronological work is necessary. Jace Koger's MSc thesis, which is the foundation of this paper, takes a general crack at the paragenetic history based on field and microscopic relationships, but we prefer to hold this back until more U-Th work is completed to anchor the observations.

2. Where has the strike and dip data been derived from and why is strike so clustered when the fault trace at a map scale is so variable? Does the presented data represent the mean of a larger sample set and if so how many datapoints were collected? This would provide confidence that the heterogeneity of the system had been captured. Additionally, I don't understand how a dip can be 90 ± 20 as the maximum dip is 90. I would like to see this data presented in the manuscript, potentially in stereonet form associated with the map?

Author Response:

The fault trace shown on the figures is from the Utah and Arizona Geological Survey's, available as ArcGIS layers on their websites. These databases are based on geological mapping at a variety of scales. Exposures of the main trace of the Hurricane Fault are not common and usually covered with colluvium. The fracture's that we measured are found close to the trace of the fault and are in general consistent with the map pattern, with some exceptions and variability. To depict this, a new figure (S3) is provided in the supplement that presents stereonets for each field station. This should help show how the facture patterns and fault orientation are generally similar.

Yes, 90 +/- 20 does not make any sense! This has been changed to 70 – 90 degrees.

3) I understand the more detailed field relationships were included in the supplementary information due to the focus of the paper, however, only the keenest readers will delve into this and you risk the context being lost to the majority of your readership. I suggest adding a paragraph to the main text that briefly summarises the supplementary information.

Author Response:

We have added additional details to the main text (section 4.1) that includes important contextual details from the supplemental material. Additionally, a new figure is included in this section.

Line by line comments

Throughout the text: Please can you be consistent with the capitalisation and name of the fault. Within this paragraph is it referred to as "Hurricane fault-zone", "Hurricane Fault", and "Hurricane fault zone". Due to the segmentation I would suggest fault-zone is most appropriate.

Author Response: We agree that different notation is used and that this is distracting. Looking at the various Utah and Arizona Geological Survey reports on the fault, as well as the published literature (e.g., Stewart and Taylor, 1996), it appears that the most consistent usage is "Hurricane fault". We agree that fault zone is more accurate in most locations. We have altered the text as appropriate.

L8: I've always preferred 'fault-fluid' as the deformation is required to localise the fluid flow, with fluid impacting later deformation.

Author Response: Changed to fault-fluid throughout manuscript, including the title.

L16: How are these differentiated as there errors overlap?

Author Response: Here in the abstract we are just reported the five dates and their 2 sigma errors. Later in the paper we make the argument that these are the same fluid flow event.

L17: All the data is taken from the FW, if possible in the word limit I would be explicit in this sentence.

Author Response: We added this information

L31: I fully agree but It may be worth citing a few of the seminal texts, or particular pertinent texts to this study, here to direct interest readers.

Author Response: We indicate that these will be highlighted in the next section

L32-62: This paragraph provides an important regional context that is also really important for introducing the concepts developed in the MS. I would however suggest that you split the paragraph into two- either one for each case study or a paragraph to highlight the value of studying fault-systems with ongoing fluid flow due to the tight age restraints and well defined structural evolution.

Author Response: Excellent suggestion, and we have divided the section into paragraphs

L35: With the basin-bounding nature of the Hurricane-fault I think it would be worth directing readers to work such as Johnathan Caine's work on the Dixie fault (cited in this MS) and some of the work coming out of Bergen from NW Greenland (e.g. the Pre-print in this SI -> Salomon, E., Rotevatn, A., Kristensen, T. B., Grundvåg, S.-A., Henstra, G. A., Meckler, A. N., Gerdes, A., and Albert, R.: Fault-controlled fluid circulation and diagenesis along basin bounding fault systems in rifts – insights from the East Greenland rift system, Solid Earth Discuss., https://doi.org/10.5194/se-2020-72, in review, 2020. And references therein

Author Response: These and other references have been added

L66: This sentence is incomplete/an amalgamate of two different sentences?

Author Response: Yes, this was a broken sentence and has been corrected.

L66-67: please include the lithologies and what is exposed in the HW and FW of the fault.

Author Response: This was added.

L67: please be specific here, particularly for reader who are not familiar with the geology of W. USA

Author Response: See prior response

L75-78: This reads more like and abstract and could be removed from the introduction. Instead I suggest that you signpost the specific research gap you hope to fill. Maybe something like "Our data enables us to constrain the source and ~540 ky evolution of fluid flow and fault-fluid interactions within the footwall of the Hurricane Fault-zone."

Author Response: Thank you for the suggested sentence. We have changed the last part of this paragraph.

L146: How was the degree of representation assessed? I struggled a little with understanding the outcrops from the main text alone and feel the main text sorely misses the context of field photographs, of which there are some very nice ones in the supplementary information. I strongly suggest that some of these are moved into the main text, and potentially one or two wider angle photographs included to help with contextualising the presented data. With only 6 figures and nice short nature of the MS I see no issue with adding another Figure.

Author Response: The degree of representation is subjective, based on the evidence of fault-fluid interaction at each field station. This study is the first of its kind along the Hurricane fault, so the goal was to cover as much ground as possible. We could not for example use any statistical

approaches for collecting the samples. We have added a figure (new figure 3) to the main text in section 4.1 as suggested to show some of the representative field relationships and outcrop styles.

L215: Also structural diagenesis after Laubach et al., 2010

Author Response: Yes, this is a good suggestion. Citation added

L218: best preserved or do you think it was localised within these competent lithologies? i.e. did diagenetic mechanical stratigraphy play a role in the fluid flow evolution of the fault zone?

Author Response: That is a great question. In some cases it is preservation because the fracturing is evident in the siltstones and shales, but these tend to be poorly exposed. In other cases the fracturing is apparent in all lithologies, but the calcite veining is only present in the sandstone or limestone units, so in this case in could be related to mechanical stratigraphy and/or permeability contrasts.

L217: How is damage zone and fault core constrained? I know this is not the main crucks of the paper, however, the distance that samples were taken from the fault core could impact the extracted data and overall interpretations (probably only minor in this case looking at the presented data). For reference on considering the thickness of fault zone and the bias can i suggest Shipton et al., 2019 doi: https://doi.org/10.1144/SP496-2018-161

Author Response: These are defined using the criteria in Caine et al., 2010. At most field sites, samples were collected fairly close to the main trace of the fault. Only in a few canyons that cut deeper into the footwall could the full damage zone thickness be walked and sampled. In these cases, clear evidence for fracturing and fluid flow were still closest to the fault trace (~100 m), but similarly oriented fractures and veins were observed up to 400 m from the fault trace. Some clarify text was added to the paper.

L245: What about structural relationship?

L246: Is there any visually difference between the sets? The geochemistry story is really well presented in this MS, however, I am struggling to link this in with the observed structural relationships.

Author Response: In response to both the above comments. There does not appear to be any consistent relationship between the structural data and vein type. This is consistent with our later interpretation that fluids are periodically moving along the fault zone. Also, over the history of the Hurricane fault, the regional stress field has been the same, so we probably should not expect distinctly different orientations associated with the history of vein formation.

L256-257: What about uncertainty due to fluid degassing?

Author Response: Later we discount degassing as a major process. However, degassing of the fluid (CO_2) should not significantly alter the salinity from NaCl or other dissolved salts, so its impact on the melting T would be secondary.

L261: What does aperture refer to, short axis? You mention long axis in the previous sentence, how elongate are the fluid inclusions?

Author Response: This has been corrected. We meant long axis.

L265: This depends on inclusion size, but in general i agree

Author Response: We have updated this section to discuss the impact of inclusion size on nucleation of a bubble and homogenization temperature.

L279: Do you have a field photograph of this you could add to the supplementary or main text?

Author Response: Unfortunately, this information is only in the field notes.

L317: this is fairly low for saline fluids, could they be saline influenced meteoric fluids?

Author Response: We have added to this discussion about the saline fluids and their possible origin. In

short, this is on the low side for basin brines. Certainly, meteoric water mixing with a brine can result in the observed salinities, as well as meteoric water-rock interaction along flow paths through marine units that include some evaportites.

L323: How appropriate is this for a terrane bounding setting that has had extensive volcanism? Do you have any constrains from well data? I would expect an elevated geothermal gradient.

Author Response: There are some data from geothermal exploration wells in the region. The gradients observed are mostly in the 18 – 24 °C/km, but a couple wells yielded 34 and 175 °C/km. So it is likely variable and perhaps elevated near the fault. We suggest however that the nominal gradients are probably more appropriate for the regional groundwater flow patterns.

Sommer, S. N., and Budding, K. E.: Low-temperature thermal waters in the Santa Clara and Virgin River valleys, Washington County, Utah, in: Cenozoic Geology and Geothermal Systems of Southwestern Utah, edited by: Blackett, R. E., and Moore, J., Utah Geological Association, Salt Lake City, 81-95, 1994.

L392: One thing that may be worth signposting in the introduction is the high resolution of dates that can be obtained through the study of these systems (and hence why studies such as this are so important to the community)

Author Response: Thank you for the suggestion – we have added a statement to this effect at the end of the introduction.

L441: I struggled to assess how robust this was from the presented data. The four geo-chemical set's is clear but how this fits into the field relationships is ambiguous. You only mention 2 'orientation-sets', how does cross cutting relate to these?

Author Response: We have updated the text to be more clear about these relationships.

L449: This is strongly suggested through your vein micro-structure you have presented both in the main text and the supplementary information.. this is a larger dataset and backs up the smaller dataset. I think it is worth highlighting this.
Author Response: We agree.

L454: Is it feasible to have no exhumation of the footwall? I am not sure i agree, particularly with the differential elevation observed in Fig1.

Author Response: We agree that there must be some exhumation of the footwall. The best constraint we can apply is using the incision rate of the Virgin River as a maximum – assuming the landscape is in steady state, the erosion rate might be a good measure of this (a maximum). The Virgin River has an estimated incision rate of 338 m/Myr (Walk et al., 2019), and this equates to ~180 m of incision since 540 ka. We added this information to the text to estimate the maximum of depth vein formation – it is still shallow (70 to 480 m).

L456: see point about geothermal gradient in the previous section.. does this also have implications for the published estimates at Pah Tempe?

Author Response: See prior comment on the constraints on the geothermal gradient.

L463: Mineralised breccias can also form due to rapid burial & differential fluid column height, see Peacock et al., 2019 -> https://doi.org/10.1111/ter.12371

Author Response: Thank you for this citation. Based on the geological history of the area and this fault, we do not think this process is relevant in this case.

L483: The shallow nature of this is a key point to highlight, although it will be a low estimate due to

exhumation & erosion of the FW

Author Response: We agree, and we have improved the depth estimate.

L491: This will have strongly effected the flow properties of the system.

Author Response: Text was added to highlight this.

L523: What is the grey-scale range? could you add a scale for this in the top left of the image?

Author Response: An elevation scale bar was added.

F2: I would like to see the lithologies other than the basalts either in a stratigraphic column or in the presented map. Could a colour scale for elevation be added to the figure?

Author Response: We feel that added the lithologies to this map will be too busy and render it very difficult to read, and we refer the readers to the excellent geological maps of the area that are all available on the Utah Geological Society's website, and free to download. A color scale bar for elevation was added.

F3: Generally really nice figure, however, a couple of suggested edits: 'calcite veins sets' appears to be slightly rotated? How are these slopes calculated? There appears to be a lot of scatter. What is the uncertainty in slopes?

Author Response: Thank you! The slopes were determined by linear regression. Agreed, there is a fair amount of scatter, and we have added the r^2 values to the plot to help quantify this.

F4: (inset) It appears the frequency does not match the presented n values? Is there not 7 results presented for set 1 & 37 for Set 3.

Author Response: Correct! We fixed the figure.

F5: The text size for the lithologies are too small

Author Response: The text size was increased

Supplementary information

FS1: (1) What are these two EW trending black lines referring to? The state boundary? (2) The text size for the segments are inconsistent (3) is the fault trace truly contentious?

Author Response: Those E-W lines were errors in the figure and have been corrected. The text size has been fixed. To the north the Hurricane fault trace is less distinct and smaller faults step over to the East.

FS2: (1) Section boundary out of alignment with the figure below, i suggest shrinking the formation column slightly to give more space for the text in the member column, (2) At several points the variable text size impacts the readability of the figure. Additionally "THICKNESS" and "LITHOLOGY" should not be in full capitals. Being slightly unfamiliar with the local geology I'd have liked to the stratigraphic column in the main text to aid broader context. It could be combined with Figure 2? (3) The schematic log needs a key & grain size scale. (4) Capitalisation is missing for several Geological members (e.g. Upper Red Member)

Author Response: We have revised this figure significantly. In fact, we have simplified the figure because it included unnecessary detail that is not discussed in the paper. This figure is just to

provide some context for the readers, but it is beyond the scope of this paper to recast the excellent geological mapping that has occurred in the area and is readily available.

L13-14: This sentence is a little clunky, consider revising

Author Response: Fixed.

L14: Could you please present the kinematic data for the described structures either in the main text or supplementary information? How many sets and what type of sets (age, chemical, orientation)?

Author Response: A new figure is included in the supplement with the vein and fracture orientations.

L15: Please also check the fault name is consistent in the supplementary information and figures.

Author Response: The supplement was updated for consistency.

L16: what proportion of the samples/studied structures?

Author Response: Probably 70%

L31: How continuous are the fault breccias?

Author Response: It depends on the location. There are some exposures where the fault breccias are continuous over 100's of meters, and in other locations very localized.

L36: what is the spatial distribution of these cemented breccias relative to the main fault?

Author Response: Based on the data we have, we cannot quantify this across the whole study area. Where we have observations, the breccias are either directly associated with the main fault trace or are within several meters.

L39: It would be good to see the lineation data preserved on these. Is there any variability between layers? purely extensional or is there a dip-slip component? How variable is the kinematic data across the different sites?

Author Response: We only have limited data on the slip surfaces.

FS3: This figure is nice and provides some of the structural context that was missing in the main text. However, could the orientation of the field photographs please be included in the figure. For clarity a scale bar could be useful (or a mention of the length of your scales in the figure caption). Also the lettering needs to be aligned with each other. In (f) mineralisation appears to be tracing along pre-existing structures here. I think a clear differentiation between 'age' sets defined by geochronology and geochemistry and 'orientation sets' needs to be woven into the manuscript.

Author Response: The figure has been edited and some of this content is now in the main text. With respect the last sentence, we feel that we have differentiated between relationships constrained by geochronology versus those based on observed cross-cutting relationships.

FS4: Please align lettering and similar to the previous supplementary figure please add in a scale bar and orientation to the field photographs

Author Response: The figure has been modified to adjust the lettering. These are unoriented photos, and include some common objects for scale in the photos.

L48: What is the type of fault breccia?

Author Response: We did not classify the fault breccias we observed.

L54: Do you have an appreciation of the relative timing of this alteration? is it recent GW circulation or related to the mineralisation? Is it preferentially related to specific fracture sets and/or orientations?

Author Response: This is a good question. Given that the reducing fluids are needed to bleach these zones, we do not think they are related to recent groundwater circulation. This alteration is most common closest to the main fault trace, associated mostly with the ~N-S oriented fractures.

Review by Matthew Steele-MacInnis

I read the paper by Koger and Newell with interest. In my opinion, the motivation is clearly articulated, the data appear robust, and the interpretations seem sound. I recommend publication with only minor revisions.

Main comment:

My only real "main" comment is related to the origin of the saline brine. Around lines 320-326, the authors suggest that the brine originated as meteoric water, which circulated deep and acquired a high solute load. Perhaps. But there seem to be other possibilities, and I'm not sure why they are not discussed. If the source of the salinity is thought to be marine sediments, then why shouldn't we consider paleo-seawater- derived brine as a possibility? In many cases, halogen compositions of basinal brines show evidence of salinity acquired by partial evaporation of seawater. I'm not saying this is the case here; just that it could be permissible, as far as I can tell. The authors may wish to check the papers by Bruce Yardley on this subject, and may also wish to expand the discussion of where these brines may have originated. Or, if other lines of evidence argue against something like this, then please explain that here?

Author response:

We agree that other sources of salinity are a possibility and we only provide our preferred interpretation. Certainly, the δ18O and moderate salinity of our most saline endmember could represent some fraction of a paleo-seawater derived brine. Unfortunately, we do not have halogen data (e.g., Cl/Br) available from our samples, and these data are not published for the thermal springs along the Hurricane fault (Pah Tempe, Travertine Grotto) that could help with fingerprinting the source. Thus with the available data we cannot distinguish between meteoric water mixing with evolved paleo-seawater or meteoric-water-rock interaction.

As the reviewer points out in comment #1, the relatively low salinity (11 wt %), although within the range observed for basinal brines, is on the low end, and thus our dataset may not capture the saline endmember. We agree that our mixing trend in Figure 6 could extend to higher salinity, higher δ18O values.

We have updated our discussion to address the other possible interpretations.

And related to this previous point, a couple smaller comments:

1) The salinity of 11 wt% NaCl is on the low end for basinal brines. This might actually be an (equivocal) argument in favor of the brine representing original meteoric water that has picked up some solutes, though I would be wary of over-interpreting this. Basinal brines generally show salinities from 5 to >30 wt%, and our large dataset from MVT deposits shows a prominent mode around 20 wt% (Bodnar et al., 2014, TOG). 11 wt% is certainly permissible for a basinal brine, just it might be worth noting that such

brines can be more saline, and this may even suggest that the true basinal “end member” has not been sampled here.

Author response: See our response to the above “main comment”.

2) Basinal brines are commonly enriched in Ca, which gives rise to first-melting tem- peratures around -50°C. Was first melting truly never observed in this study? That is a bit unfortunate, though I guess “it is what it is.” Still, I would ask you to revisit your notebooks and have a look for any notes you may have made about first melting, even if only for a few inclusions. Also, calcic brines commonly show a characteristic “orange peel” texture when frozen (Schlegel et al., 2012). Was anything like this observed?

Author response:

During the fluid inclusion measurements, we looked very carefully for first melting, and it was not observed. Also, we were not aware of the “orange peel” texture at the time of analysis; however, we did not note any unusual textures during freezing. Perhaps future work on these samples could utilize other methods to address the actual composition of the fluid inclusions (such as Raman work).

These two latter comments are obviously little things, not crucial, but might help bolster your arguments about the brine and fluid mixing.

Detailed comments:

L11: constrains

Author response: corrected

Around L170: I suggest adding a sentence or two explaining that stretching of the fluid inclusions should have no effect on the measured Tm,ice, because stretching does not modify the composition. BUT, if the inclusions underwent any degree of leakage, then this would render the observed melting T’s uninterpretable (owing to unknown degrees of H2O loss, which previous studies have shown to occur preferentially when inclu- sions partially leak). Hence, I assume that you did careful petrographic examination to confirm that there was no evidence of partial leakage. This should probably be stated.

Author response: This is a good point, and the text has been revised to include this discussion.

L220: A very minor comment, but it is awkward phrasing to say that “Secondary min- erals include primarily...” I suggest to re-word

Author response: We reworded this sentence.

L261: I do not understand this sentence: “Where present, single-phase fluid inclusion aperture is <15 μm.” Please rephrase and clarify.

Author response: This sentence was rewritten for clarity.

L265: “are generally inferred as <50 °C” – This is a bit misleading. Nucleation of vapor bubbles in high-

density inclusions definitely depends on inclusion size (smaller inclusions are more likely to be monophase), and even inclusions with nominal Th as high as 150°C sometimes fail to nucleate bubbles. The relationship with inclusion size should be noted here, and I would shy away from setting a rigid threshold at 50°C.

Author response: Thank you for pointing this out; the text has been modified to include this information.

I would delete Eq2 and the sentence that precedes it. Just say that salinity wascalcu- lated using the equation of Bodnar '93.

Author response: We have changed the sentence as suggested and removed the equation.

L305: are used to estimate (not "are used to estimatesof")

Author response: corrected

Around line 315: This is nice – the crux of the paper.

Author response: We agree, thank you.

Around line 325: See my "main" comment above.

Author response: See above discussion.

L327: Personally, I would use the term "meteoric water," instead of "meteoric groundwa- ter." Simply because the term "groundwater" is sometimes used interchangeably with basinal or connate water. I'm not advocating for that (I find that even more confusing but just for clarity and to avoid confusion, why not "meteoric water?"

Author response:Where appropriate, we have changed meteoric groundwater to meteoric water.

Around line 425: Don't your fluid inclusion observations provide an additional argument against a role of CO_2 degassing? Because of course, if CO_2 degassing was occurring, you ought to find vapor-rich inclusions dominated by CO_2. From what I can tell, there is no evidence of free CO_2 in your dataset, right? Maybe worth mentioning.

Author response: This is a good point. We do not observe any vapor dominated fluid inclusions. We have added this detail to the discussion.

Spatiotemporal history of fault-fluid interaction in the Hurricane fault, western USA

Jace M. Koger[1] and Dennis L. Newell[1]

[1]Department of Geosciences, Utah State University, Logan, UT 84322, USA

Correspondence to: Dennis L. Newell (dennis.newell@usu.edu)

Abstract. The Hurricane fault is a ~250-km-long, west-dipping, segmented normal fault zone located along the transition between the Colorado Plateau and Basin and Range tectonic provinces, western U.S. Extensive evidence of fault-fluid interaction, include, calcite mineralization and veining. Calcite vein carbon ($\delta^{13}C_{VPDB}$) and oxygen ($\delta^{18}O_{VPDB}$) stable isotope ratios range from -4.5 to 3.8 ‰ and -22.1 to -1.1 ‰, respectively. Fluid inclusion microthermometry constrains paleofluid temperatures and salinities from 45–160 °C and 1.4–11.0 wt % as NaCl, respectively. These data suggest mixing between two primary fluid sources including infiltrating meteoric water (70 ± 10 °C ,~1.5 wt % NaCl, $\delta^{18}O_{SMOW}$ ~-10 ‰) and sedimentary brine (100 ± 25 °C, ~11 wt % NaCl, $\delta^{18}O_{SMOW}$ ~5 ‰). Interpreted carbon sources include crustal- or magmatic-derived CO_2, carbonate bedrock, and hydrocarbons. U-Th dates from 5 calcite vein samples indicates punctuated fluid-flow and fracture healing at 539 ± 10.8 (1-sigma), 287.9 ± 5.8, 86.2 ± 1.7, and 86.0 ± 0.2 ka in the upper 500 m of the crust. Collectively, data predominantly from the footwall damage zone imply that the Hurricane fault imparts a strong influence on regional flow of crustal fluids, and that the formation of veins in the shallow parts of the fault damage zone has important implications for the evolution of fault strength and permeability.

1 Introduction

Secondary mineralization, alteration products, and associated textures in fault rocks provide windows into past fault-fluid interaction in the crust. Fracture networks and associated sealing cements are widely recognized not only for their tectonic significance, but also for their impact on fluid movement and distribution in the crust of groundwater, hydrocarbons, and ore-deposits (Mozley and Goodwin, 1995; Benedicto et al., 2008; Caine and Minor, 2009; Eichhubl et al., 2009; Caine et al., 2010; Cao et al., 2010; Laubach et al., 2019). The rates, spatiotemporal evolution, and mineralogy of fracture sealing cements in fault zones control fault-zone strength, the buildup of pore-pressures, location and frequency of failure events, and the overall fault system architecture through time (e.g., Caine et al., 1996; Evans et al., 1997; Sibson, 2000). In order to constrain fault-fluid interaction during and after fault slip, we need to understand the sources of fluids moving through the systems, their temperature and chemistry, and the age of fracture in-filling minerals that aid in their healing. As highlighted in the next section, the microscopy, geochronology, stable and radiogenic isotope geochemistry, bulk-rock and micro-scale geochemistry, and fluid inclusion analysis of diagenetic products in fault zones collectively inform these processes.

Deleted: fluid-
Deleted: zone
Deleted: F
Deleted: in the
Deleted: fluid-
Deleted: ing
Deleted: , occur in the footwall damage zone
Deleted: identify
Deleted: ground
Deleted: 3
Deleted: the
Deleted: F
Deleted:
Deleted: the history of
Deleted: –fault
Deleted: The f
Deleted: associated faults
Deleted: patterns
Deleted: fluid-
Deleted: need information on
Deleted: M

Exhumed brittle faults and fault damage zones are excellent natural laboratories for interpreting the interaction between fluids and faults with implications for fault-zone permeability evolution, diagenesis, and the seismic cycle (e.g., Chester et al., 1993; Caine et al., 1996; Sibson, 1996; Caine et al., 2010; Mozafari et al., 2015; Salomon et al., 2020). Our research presented here is inspired by prior studies on exhumed normal faults in the western U.S., some of which are briefly highlighted below. Although we note that many excellent examples exist worldwide in settings such as the Apennines (e.g., Ghisetti et al., 2001; Smeraglia et al., 2018), Greenland (Salomon et al., 2020), and the Dead Sea (Nuriel et al., 2012). A common theme amongst these studies is the analyses of secondary carbonate cements and fracture filling veins. Carbonate mineralization is amenable to radiogenic and stable isotopic analyses, whole-rock elemental analysis, fluid inclusion work, and dating, which allows for interpretation of past fluid temperature, chemistry, sources, and timing of fluid flow in faults. For example, the Moab Fault located in the northeastern Colorado Plateau is a world-class natural analog for the interplay between hydrocarbon-bearing fluid movement, and permeability evolution along a fault zone (Foxford et al., 1998). This east dipping normal fault exhibits a protracted history of fluid-fault interaction including hydrocarbon residues, and carbonate, oxide, and siliceous diagenetic cements and veins associated with deformation features. A suite of prior studies interprets multiple episodes fluid migration and fault-rock diagenesis between the Permian and late Tertiary due to fluid expulsion from the Ancestral Rockies Paradox Basin, during Laramide deformation, and during post-Laramide extension and exhumation (Chan et al., 2000; Chan et al., 2001; Eichhubl et al., 2009; Bergman et al., 2013; Hodson et al., 2016).

Also located in the Colorado Plateau, the Little Grand Wash and Salt Wash faults are well-exposed examples of carbonate-cemented normal fault zones that are associated with modern day spring emanations and are instructive as natural analogs for geological carbon sequestration (Shipton et al., 2004). Here extensive carbonate veins, travertine spring mounds, and CO_2-rich springs and a CO_2 geyser (Crystal Geyser) are associated with normal faulting that taps a CO_2-rich fluid reservoir at depth. Fault slip, fracturing, and subsequent sealing via carbonate mineralization are interpreted to be linked to fluid pressure build-up and release. The cycle of fault slip and sealing is related to the rate of fracture filling (Frery et al., 2015), and may also be linked to changes in hydraulic head related to glacial-interglacial climatic fluctuations (Kampman et al., 2012).

To the east of the Colorado Plateau, along the Rio Grande rift, exhumed basin-bounding and intra-basin normal faults preserve a record of syntectonic changes to fault zone permeability due to groundwater flow and mineralization in poorly lithified siliciclastic sediments (Mozley and Goodwin, 1995; Heynekamp et al., 1999; Caine and Minor, 2009; Williams et al., 2015). These studies document progressive fluid-flow localized along faults due to deformation and carbonate cementation that result in compartmentalization of basin hosted aquifers. Recent work on the Loma Blanca fault, in the south-central Rio Grande rift, documents periodic fault-slip and calcite sealing using microscopy, isotope geochemistry, and U-Th geochronology (Williams et al., 2017a; Williams et al., 2017b; Williams et al., 2019). These studies suggest that deeply circulated, CO_2-rich fluids are focused up along this fault, and that the temporal record of calcite vein fills is linked to the earthquake cycle and fault-valve behavior in this part of the Rio Grande rift.

Deleted: that also

Deleted: serve

Deleted: focusing

In this contribution, we present new results documenting paleofluid-fault interaction along the Hurricane fault zone, located at the transition between the Colorado Plateau and Basin and Range tectonic provinces of the western U.S. (Fig. 1). The Hurricane fault juxtaposes Mesozoic and Paleozoic carbonates, sandstones, and shales along its strike, with excellent exposures of the footwall. Also proximal to and offset by the Hurricane fault are Pliocene – Pleistocene volcanic centers and basalt flows that may have periodically influenced the fluid-flow and thermal regime near the fault (Fig. 2). Prior research on the Hurricane fault has focused primarily on its structural and paleoseismic history (Stewart and Taylor, 1996; Fenton et al., 2001; Lund et al., 2007), with studies on fault-fluid interaction limited to modern thermal springs (Crossey et al., 2009; Nelson et al., 2009). We present the first quantitative results on the spatiotemporal thermochemical evolution of paleofluid flow and fluid-rock interaction along the Hurricane fault zone using stable isotope geochemistry, fluid-inclusion microthermometry, and U-Th geochronology of calcite vein networks exposed in the footwall damage zone. Our data enables us to constrain the sources and approximately 540 ka evolution of fluid flow and fault-fluid interactions within the footwall of the Hurricane fault zone, and this study highlights the value of integrating relatively high-resolution U-Th dates with other geochemical data from fault-hosted calcite veins.

2 Geological Setting of the Hurricane fault zone

The Hurricane fault zone strikes roughly north-south in the transition zone between the Colorado Plateau and the Basin and Range tectonic provinces in southwest Utah and northwest Arizona (Fig. 1). Major tectonic events that have shaped the region include the Sevier orogeny, Laramide orogeny, and subsequent Basin and Range extension. The Sevier orogeny and associated fold and thrust belt initiated at ~125 Ma due to subduction and formation of a continental arc along the western margin of North America (Armstrong, 1968; Heller et al., 1986). The fold and thrust belt progressed eastward until shallowing of the subducting Farallon slab marked the onset of the Laramide orogeny at ca. 75 Ma (Livaccari, 1991; Yonkee and Weil, 2015). Laramide deformation is marked by basement-cored uplifts and the formation of the Rocky Mountains. Hydration of the continental lithosphere during this time lab led to widespread magmatism following foundering of the Farallon slab (Humphreys et al., 2003). Basin and Range extension and wide-spread normal faulting in the western U.S. began in the late Eocene (Axen et al., 1993).

Normal faults of the Basin and Range broadly follow Proterozoic accretionary and Sevier-Laramide compressional structural fabrics to accommodate late Paleogene extension (Armstrong, 1968; Quigley et al., 2002). Extension along the eastern margin of the Basin and Range adjacent to the Colorado Plateau initiated ~ 15 Ma (Axen et al., 1993). The Colorado Plateau province has remained largely un-deformed by Basin and Range extension, and the transition from the thick, strong crust of the Colorado Plateau to the relatively thin crust of the Basin and Range occurs over a ~ 100-km-wide interval (Zandt et al., 1995). The eastern margin of the transition zone is also coincident with the Intermountain Seismic Belt, (Fig. 1), with multiple seismically active normal faults including the Wasatch and Hurricane fault zones (Smith et al., 1989). Late Cenozoic volcanism along the margin between the two tectonic provinces is compositionally bimodal, indicative of high heat flow and partial melting of the mantle (Best and Brimhall, 1974).

Deleted: -
Deleted: F
Deleted: is major, segmented, and seismically active normal fault located
Deleted: ing
Deleted: sedimentary
Deleted: rocks
Deleted: damage zone
Deleted: F
Deleted: altered
Deleted: fluid-fault
Deleted: history
Deleted: Geochemical data indicate that the paleofluids migrating along the fault were mixtures of deeply circulated meteoric water and sedimentary brines with contributions from hydrocarbons and possibly recent magmatism. Textural and preliminary geochronological results from veins suggest punctuated fluid flow and fracture sealing events, possibly associated with fault slip along the Hurricane Fault.
Deleted: F
Deleted: F
Deleted: The
Deleted: event
Deleted: inititated

The Hurricane fault is a 250-km long, segmented, west dipping normal fault in southwestern Utah and northwestern Arizona with poorly constrained origins in the mid-Miocene to Pliocene (Lund et al., 2007; Biek et al., 2010). Fault activity occurred predominantly in the Pleistocene, including up to 550 m of its total 600–850 m of throw (Lund et al., 2007). Six segments of the Hurricane fault are 30–40 km long and have been defined based on geometric and structural complexities at segmentation boundaries (Fig. S1) (Pearthree et al., 1983; Stewart and Taylor, 1996; Stenner and Pearthree, 1999). The Hurricane fault is recently active as evidenced by Quaternary scarps, and the magnitude ~5.8 earthquake occurring in 1992 east of St. George, Utah with a focus at ~15 km depth along the projected dip of the Hurricane fault surface (Stewart and Taylor, 1996). Long-term slip rates based on paleoseismic studies range from 0.44 to 0.57 mm/y (Lund et al., 2007).

Rock types juxtaposed by the fault include Paleozoic and Mesozoic sandstones, siltstones and mudstones, marine limestones, and evaporites (Biek, 2003; Biek et al., 2010). Exposures of hanging wall bedrock are broadly covered by Quaternary colluvium concealing Triassic units that are exposed in a few locations. Permian and Triassic units are well exposed in the footwall along the Hurricane cliffs, especially in canyons cutting the escarpment (Fig. S2). Units dominated by marine carbonates include the Permian Pakoon Dolomite, Permian Toroweap Formation, and Permian Kaibab Formation, and lower members of the Triassic Moenkopi Formation. Siliciclastic-dominated units in footwall exposures include the Permian Queantoweap Sandstone (stratigraphically equivalent to the Hermit Formation along the southern segments of the fault), and Triassic Moenkopi Formation. Where exposed along the fault, the Permian Queantoweap Sandstone and Hermit Formation are composed of very fine to fine-grained quartz-rich sandstone, locally cemented by calcite and/or silica and hematite.

Basaltic volcanism in the eastern Basin and Range in the transition zone to the Colorado Plateau began at ~15 Ma and has been most active within the last 2.5 My (Nelson and Tingey, 1997). Quaternary basaltic volcanic centers are spatially associated with the Hurricane fault (Fig. 2). Basalt flows are offset by the Hurricane faults, and these are used for constraining long-term slip rates (Lund et al., 2007). Volcanic eruptions are predominantly alkali-rich basalts with lesser basaltic andesite. Neodymium isotope ratios of Quaternary basalts reflect primarily lithosphere sources along the northern half of the Hurricane fault and asthenosphere/mixed source to the south (Crow et al., 2011). These periods of basaltic magmatism associated with Basin and Range extension may have created hydrothermal systems in the past that locally influenced groundwater chemistry and circulation in the Hurricane fault.

Prior work on fluid movement associated with this fault is limited to geochemical and isotopic studies of modern spring systems at Pah Tempe hot spring, near La Verkin, UT, and the Travertine Grotto and Pumpkin warm springs in Grand Canyon. At Pah Tempe hot spring, deeply-circulated meteoric waters emerge as CO_2-charged and saline fluids along the fault trace, and precipitation of calcite veins is evident in the exhumed fault rocks (Nelson et al., 2009). Travertine Grotto and Pumpkin warm springs are attributed to meteoric water mixing with deeply-sourced fluids that are flowing upwards along the basement-rooted Hurricane fault (Crossey et al., 2006; Crossey et al., 2009). Analyses

Deleted: F
Deleted: vertical displacement
Deleted: F
Deleted: and Hermit Formation
Deleted: The Permian Hermit Formation includes fine-grained quartz-rich sandstones with minor hematite and calcite cements.
Deleted: is
Deleted: quartz
Deleted: F
Deleted: F
Deleted: F

of volatiles exsolving from these springs identifies a predominantly deep (endogenic) source, with some modern contributions from mantle or magmatic sources.

3 Methods

3.1 Field Locations

Field investigations along the Hurricane fault were conducted between Cedar City, UT and the fault's intersection with Grand Canyon in Arizona (Fig. 2). Studies were restricted to well-exposed areas of the fault's footwall, typically where canyons and drainages cross the fault. Due to colluvial cover on the hanging wall, this study focused on footwall exposures of the fault and the footwall damage zone. Twenty-three field stations (Fig. 2) along Hurricane fault were investigated, and hand samples were chosen for subsequent microscopic and geochemical characterization of diagenetic alteration and secondary vein mineralization. Sampling criteria included vein morphology, cross-cutting vein relationships, varying vein/fracture orientations, and range of apparent diagenetic modification, including unaltered host rocks. The goal was to collect a representative suite of hand samples at each of the 23 field stations to capture the range of fault-fluid interaction observable over ~160 km of fault length. Sample locations were recorded using a Garmin™ GPS unit in decimal degrees relative to the WGS 1984 datum (Table S1). Fracture intensity (fractures per meter) in the footwall exposures were measured at each field station using linear scan line methods (e.g., Watkins et al., 2015). Fracture distance from fault and orientation was recorded for fractures intersecting a measuring tape oriented roughly orthogonal to the fault trace. Scan line lengths were variable due to available field exposures and ranged from <10 m to ~400 m.

3.2 Microscopy

Standard petrographic thin sections were made from 34 hand samples displaying a range of vein types and diagenetic alteration. Of these 34 samples, 15 doubly-polished thick sections (150-um-thick) of calcite veins were prepared for fluid inclusion analyses. Thin section petrographic observations were made using Leica Z16 APO and Leica DM 2700P petrographic microscopes. Photomicrograph images were acquired with a Leica MC 170 HD camera and processed using the Leica Application Suite 4.6 software.

3.3 Fluid inclusion microthermometry

Fluid inclusions in secondary calcite mineralization were investigated using a Zeiss Universal transmitted light microscope with a Zeiss Epiplan 50x long-working distance objective. A USGS gas-flow heating and freezing stage was used to measure fluid inclusion homogenization and melting temperatures. The stage was calibrated to the critical point of water using a synthetic supercritical H_2O inclusion (374.1 °C), the freezing point of a synthetic 25 mol % CO_2-H_2O inclusion (-56.6 °C), and the freezing point of double-deionized water using an ice bath (0 °C). Using the 15 thick sections, 107 homogenization temperatures (T_h) and 35 melting temperatures (T_m) were determined from two-phase fluid inclusions in calcite (Table 1).

Deleted: ¶
Deleted: F
Deleted:
Deleted: zone
Deleted:
Deleted: F
Deleted: representative
Deleted: petrographic
Deleted:
Deleted:

Fluid inclusion were classified and homogenization and melting temperatures were determined using criteria and procedures described by Goldstein and Reynolds (1994) and Goldstein (2001). After performing heating measurements, numerous 2-phase fluid inclusions with homogenization temperatures from 45 – 85 °C became metastable 1-phase liquid inclusions (i.e., the bubble did not re-nucleate upon cooling). In order to re-nucleate the second phase to facilitate measuring the melting temperatures, these fluid inclusions in these samples were intentionally stretched by heating to 110 °C for 18 hours in a laboratory oven (Goldstein and Reynolds, 1994). Stretching does not impact the melting temperature because it does not alter the inclusion composition. However, if the inclusion is damaged during stretching, resulting in some water leakage, this could render melting temperatures meaningless. For a few of these treated inclusions, unreliable melting temperatures >0 °C were obtained, and these were omitted from the data set. It is possible that stretching induced leakage from these inclusions, although this was not observed during petrographic observations. No pressure correction was performed to convert T_h measurements to trapping temperatures (T_t). Assuming vein formation at a maximum depth of 800 m equivalent to the maximum throw on the fault (Anderson and Mehnert, 1976), a maximum pressure using a lithostatic load (2675 kg m^{-3} rock density), and the maximum measured T_h of 160 °C, the pressure correction is <10 °C (Fisher, 1976; Bakker, 2003) and considered insignificant for this study. T_h measurements in this study are considered representative of T_t.

3.4 Carbon and oxygen stable isotope analysis

A Dremel® tool was used to collect 290 powdered sub-samples from calcite veins, mineralized fracture surfaces, limestone host rock, and calcite-cemented sandstone host rock. Carbon and oxygen stable isotope analyses of these samples was performed in the Utah State University Department of Geosciences Stable Isotope Laboratory using a Thermo Scientific Delta V Advantage Isotope Ratio Mass Spectrometer (IRMS) and a GasBench II using the carbonate-phosphoric acid digestion method (McCrea, 1950; Kim et al., 2015). Specifically, ~ 120-150 µg aliquots of relatively pure calcite samples and standards were placed into 12 ml Exetainer© vials and flushed with ultra-high-purity helium. Impure carbonate cements (e.g., calcite-cemented sandstone) required 300 to 8000 µg of sample to achieve acceptable peak amplitudes during analysis. After helium flushing, ~ 100 µL of anhydrous phosphoric acid was added to each sample and allowed to react for two hours at 50 °C before analysis. Carbon and oxygen stable isotope ratios were calibrated and normalized to the VPDB scale using the NBS-19 and LSVEC, and NBS-19 and NBS-18 international standards, respectively (Kim et al., 2015). In house calcite standards were used to correct for drift and mass effects. Carbon and oxygen isotope ratios are reported using delta notation ($\delta^{13}C$, $\delta^{18}O$ values) in per mil (‰) relative to VPDB. Based on repeat analyses of in-house calcite standards, errors on $\delta^{13}C$ and $\delta^{18}O$ values are <0.1 ‰. Oxygen isotope ratios are also converted and reported relative to standard mean ocean water (SMOW) for fluid inclusion calculations using Eq. (1) (Sharp, 2007):

$$\delta^{18}O_{SMOW} = 1.03091 * \delta^{18}O_{VPDB} + 30.91 \quad \text{Eq. (1)}$$

Deleted: ¶

3.5 Uranium-thorium (U-Th) dating

Pilot U-Th geochronology was conducted on 5 key calcite vein samples from two field locations (Table S2). These include locations 1-2 and 1-4, where veins are hosted in limestone and sandstone strata, respectively (Fig. 2). Veins

were slabbed with a rock saw and approximately 300 mg of calcite powder was collected from discrete veins or vein laminations using a Dremel® tool and submitted to the University of Utah ICP-MS laboratory for analyses. At location 1-2, one laminated vein was subsampled at two locations (one near vein wall and near the outer part of the vein) to capture the timing of vein growth. At location 1-4, 3 generations of veins, determined based on cross-cutting relationships, were subsampled.

Chemical preparation and analyses were performed at the University of Utah following methods modified from Edwards et al. (1987) using a Thermo NEPTUNE Plus Multi-Collector-Inductively-Coupled-Mass-Spectrometer (MC-ICP-MS). Powdered carbonate samples were dissolved in 16 M HNO_3 and equilibrated with a mixed ^{229}Th-^{233}U-^{236}U spike and refluxed on heat for at least one hour to ensure total dissolution. Uranium and thorium sample fractions were separated for analyses by anion exchange column chemistry. Measured peak heights were corrected for abundance sensitivities and mass bias, dark noise, background (blank) intensities, hydride contributions, ion-counter yields, and spike contamination. The spike was calibrated against solutions of CRM 145 and HU1 uraninite. Uncorrected age uncertainties are reported as one standard error and include measurement error and uncertainties of activity. Details of the spike calibration and data treatment can be found in Quirk et al. (2020).

Deleted: (in review)

4 Results

4.1 Fault zone diagenesis and veins

Evidence for fluid-fault interaction along Hurricane fault zone exists at the macroscopic and microscopic scale. Collectively referred to as "fault zone diagenesis" (Knipe, 1992) and "structural diagenesis" (Laubach et al., 2010), these observations form the foundation for subsequent geochemical and geochronological work. Examination of the fault zone exposures at the 23 field sites (Fig. 2) reveals that it is composed of a up to 400-m-wide damage zone. The damage zone (e.g., Caine et al., 1996) was qualitatively defined as the part of the exposed footwall away (east) from the main fault trace that exhibits minor slip surfaces, deformation bands, and is more intensely fractured than the unaltered host rock. We acknowledge that our assessment of the damage zone thickness is limited to the observed and available fault exposures. Exposures of the fault core (e.g., Caine et al., 1996) are less common and range from 0.5 m to 2 m thick, characterized by fault breccia and gouge zones, often bounded by large slip surfaces. The record of paleofluid flow and deformation is best preserved in competent sandstone and limestone units within the damage zone, rather than finer grained units that are typically poorly exposed. Evidence for chemical and mechanical fluid-rock interaction includes host rock alteration, veins, and mineralized/cemented slip surfaces, deformation bands, and breccias (e.g., Fig 3). Secondary minerals include calcite, with lesser hematite, manganese oxides, and gypsum. Reduction (e.g., "bleaching" of sandstones, Fig. 3 a, b) and oxidation features are observed in siltstone and sandstone strata with calcite and iron oxide cements. Manganese and iron-oxide vein cements, and brecciated veins are primarily observed in sandstone strata. Sparry calcite veins are the most common feature in limestone strata, with nearly every fracture hosting some calcite mineralization. The calcite veins range from single generation mm- to cm-scale sparry fracture fills to cm-scale laminated and fibrous veins with clear crystal terminations. Vein walls comprise intact host

Deleted: ~10 to
Deleted: ,
Deleted: and f
Deleted:
Deleted: primarily
Deleted: (redox)

rocks (limestone and sandstone) and calcite-cemented breccia. Diagenetic products are most commonly associated with zones of more intense fracturing, although veins occur throughout the damage zone.

Fracture intensity varies from ~2 to 20 m^{-1} within the Hurricane fault's damage zone. Intensely fractured zones (or corridors) of 10–20 m^{-1} are 1–2 m wide and are pervasively mineralized and "bleached" if cutting hematite-cemented sandstone. Bleaching removes hematite quartz coatings, leaving white to tan coloration in contrast to the surrounding red sandstone. Fracture orientations typically follow two main sets: one striking 0 ± 10°, and one 300 ± 15°, both dipping-steeply 70 to 90° (Fig. S3). The approximately north striking fractures are generally similar to the map-scale trend of the Hurricane fault. Please refer to the supplemental documentation for more descriptions and photos of the observed veins, features associated with fault slip, and alteration of the host rocks (Figs. S4 – S6).

Deleted: dense
Deleted: sparse
Deleted:
Deleted: density
Deleted: F
Deleted: Densely
Deleted: sub-parallel to the fault trace
Deleted: 90 ± 20
Deleted: 3
Deleted: 5

4.2 Vein geochemistry

4.2.1 Carbon and Oxygen stable isotope ratios

Stable isotope ratios of carbon and oxygen were determined for calcite veins and host rocks from the field sites (see data repository, Newell and Koger, 2020). The $\delta^{13}C_{VPDB}$ and $\delta^{18}O_{VPDB}$ values for the entire data set range from -4.5 to 3.8 ‰ and -22.1 to -1.1 ‰ (8.1 to 29.8 ‰ vs SMOW), respectively (Fig. 4 a). In the host rock units, carbonate cements in siliciclastic units and bulk limestone host-rock were analysed adjacent to veins and at ~ 1–2 m away for comparison. Host rocks near fractures have $\delta^{13}C_{VPDB}$ and $\delta^{18}O_{VPDB}$ values from -4.5 to 2.8 ‰ and -17.7 to -8.6 ‰, respectively. Away from fractures, host rock $\delta^{13}C_{VPDB}$ and $\delta^{18}O_{VPDB}$ values range from -2.0 to 3.8 ‰ and -8.5 to -1.1 ‰, respectively. The $\delta^{13}C$ and $\delta^{18}O$ values for calcite veins, breccia cements, mineralized fractures, and slip surface cements span a wide range of values with considerable scatter. For the purposes of presentation and discussion these data are divided into 4 "vein sets" based on common lithological associations, vein morphologic features, and $\delta^{13}C$ and $\delta^{18}O$ value data patterns (Fig. 4 a). Note that these 4 vein sets span multiple locations (Fig. S1) and show no correlation in C and O isotope ratios with location. There is no apparent relationship between vein set and orientation (Fig. S3).

Deleted: 3
Deleted: 3
Deleted:

Vein set 1 calcite exhibits a positive correlation (slope = 1.6) between $\delta^{13}C$ and $\delta^{18}O$ and is commonly intergrown with hematite when hosted in siliciclastic strata. Calcite in set 2 also displays a positive $\delta^{13}C$ and $\delta^{18}O$ correlation (slope = 0.9) with $\delta^{13}C$ shifted to lower values compared to vein Set 1. Set 3 has a wide range of isotopic values, showing no strong trends or patterns. Set 4 calcite $\delta^{18}O$ values that overlap with set 3 with $\delta^{13}C$ values that trend to significantly lower values. The majority of set 4 data are from location (1-2).

4.2.2 Fluid inclusion microthermometry

Of the 15 thick sections of calcite veins observed, 6 contain populations of two-phase fluid inclusions that yield homogenization (T_h) and melting (T_m) temperatures (Table 1, Fig. 5). Homogenization temperatures are used to approximate the trapping temperature (T_t) and are representative of fluid temperatures during mineralization. Melting

Deleted: 4

temperatures depend on the nature and concentration of dissolved species and are used to estimate the salinity of paleofluids (Bodnar, 1993).

Fluid inclusion homogenization and melting temperature data is organized by the calcite vein set as described in section 4.2.1. Observed two-phase fluid inclusions range from ~5–40 µm on the long axis. Most inclusions are interpreted to be primary and there are few trails of secondary inclusions. Single-phase (water) fluid inclusions are also present with long axis dimensions <15 µm. Homogenization temperatures for set 1 two-phase inclusions range from 45–90 °C. Vein set 3 samples have two-phase fluid inclusion homogenization temperatures from 55–160 °C, and their distribution skews towards lower temperatures, with a mode at 65–70 °C. Only single-phase fluid inclusions are present in vein sets 2 and 4. Trapping temperatures for single-phase inclusions cannot be readily determined. Trapping temperatures are often inferred as <50 °C (Goldstein and Reynolds, 1994; Goldstein, 2001); however, small inclusions (<10 µm) can fail to nucleate a bubble up to ~140 °C (Krüger et al., 2007). Ice melting temperatures from vein set 1 range from -3–0 °C, equating to a salinity of 0 to 5 wt% as NaCl (Fig. 5). Calcite set 3 yield melting temperatures from -11 to 0 °C, equating to 0 to 15 wt% NaCl. Since no initial melting was observed, NaCl dominated salinity is assumed and calculated using the equation of Bodnar (1993).

4.3 U-Th geochronology

The U-Th dates from the 5 vein samples range from 86 ka to 539 ka (Table S2). More specifically, the laminated calcite vein from location 1-2, hosted in limestone strata, yields an inner lamination date of 113.1 ± 0.3 ka (1-sigma error) and an outer lamination date of 86.2 ± 1.7 ka (Fig. 6). The three calcite veins at location 1-4, hosted in sandstone strata yield dates of 539 ± 10.8 ka, 287.9 ± 5.8 ka, and 86.0 ± 0.2 ka in chronological order consistent with cross-cutting relationships. Two dates from a single sample include calcite cement from a brecciated vein wall (288 ka) that is crosscut by a laminated calcite vein (86 ka) (Fig. 6). In the field, this vein crosscuts the 539 ka vein.

5 Discussion

5.1 Paleofluid sources in the Hurricane fault

The carbon and oxygen stable isotope ratios of the calcite veins can inform the groundwater composition, source, and processes at work during paleofluid circulation in the Hurricane fault. The C and O equilibrium isotopic fractionation between CO_2 and calcite (cc) and water and calcite (cc), respectively are temperature dependent, and assuming that isotopic equilibrium during mineralization is valid, additional information on the paleofluid temperature is needed to proceed. Homogenization temperatures of primary 2-phase fluid inclusions in calcite, when present, are a reliable method to estimate temperature, and thus to calculate the paleofluid O and C isotopic composition using Eq. (2) and Eq. (3):

O isotopes: $1000ln\alpha_{H2O-cc} = 2.89 - \frac{2.78*10^6}{T^2}$ (O'Neil et al., 1969; O'Neil et al., 1975) Eq. (2)

C isotopes: $1000ln\alpha_{CO2-cc} = 3.63 - \frac{1.194*10^6}{T^2}$ (Deines et al., 1974) Eq. (3)

Deleted: Where present, si
Deleted: aperture is
Deleted: small
Deleted: are
Deleted: generally
Deleted: 4
Deleted: via Eq. (2) where T_m is the measured melting temperature in °C…
Deleted: ¶ $(wt\%\ NaCl) = 0.00 + 1.78\,T_m - 0.0442\,T_m^2 + 0.000557\,T_m^3$ → → → → → → Eq. (2)¶ ¶
Deleted: +/-
Deleted: +/
Deleted: 5
Deleted: +/-
Deleted: +/-
Deleted: +/-
Deleted: Specifically, t
Deleted: 5
Deleted: F
Deleted: 3
Deleted: 4
Deleted: 3
Deleted: 4

where $\alpha_{x\text{-}y}$ is the temperature dependent fractionation factor between water and calcite (H_2O-cc), CO_2 and calcite (CO_2-cc), and T is temperature in Kelvin. For the fractionation factor magnitudes expected for these two systems, the difference in delta values between the phases (i.e., $\delta^{18}O_{H2O}$ - $\delta^{18}O_{cc}$ and $\delta^{13}C_{CO2}$ - $\delta^{13}C_{cc}$) is a good approximation for $1000ln\alpha$ (Sharp, 2007). When fluid inclusion data are not available, temperatures may be estimated based on other constraints, such as estimates on mineralization depths and the geothermal gradient, but the resulting paleofluid isotopic estimates will be far more uncertain due to surface-ward advection of geotherms (Forster and Smith, 1989). Clumped carbonate isotopic methods (Δ_{47}) can yield reliable temperature estimates from fault-zone calcite mineralization (Swanson et al., 2012; Hodson et al., 2016), but are not available for this study. In the absence of these constraints, a range of temperatures or starting fluid isotopic compositions can be explored to provide some interpretations of the calcite stable isotope data, again resulting in considerable uncertainty.

For the 6 samples that hosted populations of two-phase fluid inclusions, microthermometry heating and freezing data are used to estimates fluid trapping temperatures and salinities of the paleofluids present in the Hurricane fault. In combination with $\delta^{18}O$ values from the calcite hosting these fluid inclusions, the paleofluid $\delta^{18}O$ values are calculated using Eq. (2). Although calcite oxygen stable isotope measurements are conducted on micro-drilled aliquots, these are still bulk samples when considering the microscopic distribution of fluid inclusions. Also, in each sample the microthermometry results yield populations of fluid inclusions with some variation in homogenization temperature. Therefore, we cannot connect individual isotopic values to individual fluid inclusions. Rather we use the mean and standard deviation of measured temperatures in each sample along with the calcite $\delta^{18}O$ value to estimate a range of paleofluid compositions (Table 1). Similarly, we associate this range of oxygen isotope values to the mean and standard deviation of the paleofluid salinity as estimated from fluid inclusion melting temperatures. The paleofluid $\delta^{18}O$ value and salinity (wt % as NaCl) estimates for these samples show a strong positive correlation (R^2 = 0.8; Fig. 7). We interpret this correlation as mixing between two endmember fluid types, and that over the history of fluid-fault interaction represented by these calcite veins, different proportions of ~100 +/- 25 °C, saline (~11 wt % NaCl), high $\delta^{18}O$ (~5 ‰) fluids have mixed with 70 +/- 10 °C lower salinity (~1.5 wt% NaCl), lower $\delta^{18}O$ (~-10 ‰) ground waters.

We suggest that the endmember characterized by high $\delta^{18}O$ values and high salinity is consistent with sedimentary formation water (brine) that originated from extensive meteoric water-rock interaction and oxygen isotope exchange with marine sedimentary sequences (e.g., Clayton et al., 1966). Assuming a 25 – 30 °C geothermal gradient and the range fluid inclusion temperatures, circulation depths for these ground waters ranges from 2 to 6 km. This geothermal gradient is consistent with most observations from geothermal exploration wells in the region (Sommer and Budding, 1994). This is adequate to infiltrate all of the Mesozoic and Paleozoic strata in the region, including thick sections of marine carbonate and evaporite bearing units (Biek, 2003; Dutson, 2005; Biek et al., 2010).

Deleted: of
Deleted: F
Deleted: oxygen stable isotope ratios
Deleted: is
Formatted: Superscript
Deleted: 3
Deleted: r
Deleted: 6

Infiltration into these marine units is a likely source for the salinity in these ground waters. The endmember characterized by relatively low-salinity and low $\delta^{18}O$ value is likely dominantly meteoric water. Using the same geothermal gradient, these ground waters have circulated to ~3.5 km based on fluid inclusion constraints. For comparison, Pah Tempe hot springs (Nelson et al., 2009), and Pumpkin and Travertine Grotto springs (Crossey et al., 2009) emanate along the Hurricane fault and have similar oxygen isotope composition and salinity to this endmember (Fig. 7). Based on comparisons of Pah Tempe hot spring $\delta^{18}O$ and $\delta^{2}H$ values with other local and regional meteoric waters, Nelson et al. (2009) interpret the source of the hot spring water as meteoric water that infiltrated during the last glacial interval. Based on geochemical geothermometry estimates, and the observed shift in hot spring water to higher $\delta^{18}O$ values, Nelson et al. (2009) suggest that Pah Tempe thermal waters circulation depths of 3-5 km with temperatures of 70-150 °C. This approach has also been employed at other faults to interpret paleofluid compositions. For example, coupled fluid inclusion microthermometry and stable isotope values from fault-hosted calcite along the Moab fault, UT, USA, point to a mixing process between upwelling basin brines with meteoric water (Eichhubl et al., 2009). Although we suggest that the saline fluids in the Hurricane fault are the product of water-rock interaction, it is important to note that an alternative interpretation is mixing between meteoric water and basin brine derived from the evaporation of paleo-seawater. The "high salinity" endmember we observe is consistent with basin brines, albeit on the low end of observed salinities (e.g., Bodnar et al., 2014). It is possible that we have not captured the true high salinity endmember in our sampling. To further evaluate the source of the saline fluids, additional data that is currently not available such as halogen content and isotopic composition (e.g., Cl/Br, $\delta^{37}Cl$ value) may be diagnostic (e.g., Yardley et al., 2000).

In terms of the carbon sources in these two fluids, there are alternative ways to interpret the relatively narrow range of calcite $\delta^{13}C$ values (0.35 to 1.73 ‰). First, using the average calcite formation temperatures from fluid inclusions, we can estimate the carbon isotopic composition of the paleofluid dissolved CO_2 from -6.1 to -4.3 ‰ (VPDB) using Eq. (3) (Table 1). However, unlike the oxygen isotope system that most likely reflects the water composition, carbon composition can be reflective of a carbonate host rock. For example, dissolved carbonate in equilibrium with limestone bedrock (i.e., strongly buffered by the host rock) will result in calcite veins with a $\delta^{13}C$ similar to the host limestone (e.g., Dietrich et al., 1983). In this case, calculating the carbon isotopic composition of and external CO_2 source may not be appropriate, and the vein value is simply representative of the source carbon. In this study, the host rock limestone $\delta^{13}C$ values range from -2.7 to 3.8 ‰ with an average of 1.2 ‰, which is in the range of expected values from marine carbonates (e.g., Hoefs, 1987; Sharp, 2007). However, in parts of the fault that have higher water-rock ratios or are generally carbonate poor (e.g., siliciclastic host rock), the carbon isotopes of calcite veins can be representative of an external CO_2 source dissolved and traveling in the groundwater. With these uncertainties in mind, we interpret the endmember carbon sources for the calcite veins as external CO_2 sources and local marine limestones. Based on the results from this study, there may be a weak association between the two carbon sources and the fluid endmembers based on oxygen isotopes and salinity. In some but not all cases, vein $\delta^{13}C$ values that are

Deleted: ground

Deleted: 6

Deleted: ally

Deleted: derived ground

Formatted: Superscript

Deleted: 4

similar to host limestone tend to be associated with the highest salinity fluids. Veins hosted in sandstone units and associated with an external CO_2 source (~-6 ‰) are in most cases associated with the lower salinity fluids. These carbon isotope values are similar to the observed $\delta^{13}C$ values of CO_2 at Pah Tempe (-5.5 ‰) and Pumpkin (-6.1 ‰) springs (Crossey et al., 2009; Nelson et al., 2009). These values overlap with mantle CO_2 values (Marty and Jambon, 1987), but are also are similar to values observed in many crustal fluids and continental hot springs globally (Sherwood Lollar et al., 1997; Ballentine et al., 2002; Newell et al., 2008; Newell et al., 2015). Based on helium and carbon isotopes, Crossey et al. (2009) and Nelson et al. (2009) suggest that mantle CO_2 could range from a just a few percent to as high as ~40 % in the Hurricane fault hosted hot springs, depending on the mantle and crustal end members used. We do not have constraints on the helium isotope ratios of the paleofluids, so we cannot further evaluate the possibility of magmatic contributions.

5.2 Subsurface processes impacting isotopic values

As shown earlier, the $\delta^{13}C$ and $\delta^{18}O$ values from calcite veins and cements associated with the Hurricane fault display a large range of values (Fig. 4 a). In addition to the binary mixing described in section 5.1, precipitation of calcite from fluids with a range of temperatures is occurring along flow paths. A fairly wide range of temperatures is evident from the fluid inclusion work on vein sets 1 and 3. For a given water $\delta^{18}O$ and $\delta^{13}C_{CO2}$, varying temperature in Eqs. (2) and (3) results in trends in calcite $\delta^{18}O$ and $\delta^{13}C$ with a slope of ~2.3 (Fig 4 b). To explore the impacts of both temperature change and mixing, the calcite forming from the saline ($\delta^{18}O_{VSMOW}$ = 5 ‰) and meteoric water ($\delta^{18}O_{VSMOW}$ = -10 ‰) endmembers, both with a $\delta^{13}C_{VPDB}$ = -6 ‰ are superimposed on the observed data (Fig. 4 b, shaded region). The vein set 1 pattern is fairly well matched by calcite forming over a the range of T consistent with the fluid inclusion measurements (90-45 °C) from the low-salinity meteoric water end member ($\delta^{18}O_{VSMOW}$ = -10 ‰ ; $\delta^{13}C_{VPDB}$ = -6 ‰). The scattered values observed for vein set 3 are encompassed by the calcite forming from mixed saline and meteoric fluids over the range of temperatures consistent with the fluid inclusion measurements (160-50 °C). Although not shown on the diagram, using a limestone-buffered $\delta^{13}C$ (~1 ‰) predicts values that are *not* consistent with any of the observed data, and this suggests that an external source of CO_2 may be most appropriate for veins in both the carbonate and siliciclastic host rock. The vein set 4 isotopic values are best explained by mixing the saline end member at ~100 °C with a $\delta^{13}C$ source of ~ -12 ‰ (Fig. 4 b). This low $\delta^{13}C$ value is consistent with derivation from organic matter (Boles et al., 2004). Hydrocarbons are present regionally and in the strata that hosts the Hurricane fault (Bahr, 1963; Blakey, 1979). Mobilization and microbial oxidation of these hydrocarbons to form dissolved carbonate (Baedecker et al., 1993; Tuccillo et al., 1999) has been shown in other fault settings to form calcite veins with low $\delta^{13}C$ values (e.g., Eichhubl et al., 2009).

Open-system processes can also result in a range of calcite O and C stable isotope values. For example, open system CO_2 degassing and calcite precipitation results in progressive fractionation of C and O stable isotopes in the fluid that result in correlations between $\delta^{13}C$ and $\delta^{18}O$ values (Hendy, 1971). Kampman et al. (2012) used a Rayleigh

Deleted: 3

Deleted: 3

Deleted: 4

Deleted: 3

Deleted: 3

Deleted: 3

fractionation model, assuming isotopic equilibrium, to describe C and O stable isotope values observed in fault-controlled aragonite veins and travertine deposits in the Salt Wash Graben, UT, USA. Here, coupled CO_2 degassing and carbonate precipitation from a homogenous CO_2-charged fluid source can explain the positive correlation and range in $\delta^{13}C$ and $\delta^{18}O$ values. In combination with U-Th geochronological constraints, these authors suggest that this system has been active periodically for >100 ky with a consistent paleofluid source and isotopic composition.

Here we test if the positively correlated C and O values observed for vein set 1 (slope = 1.6) and set 2 (slope = 0.9) (Fig 4 a) can be explained by a similar process. Rayleigh fractionation trends are included on figure 4 (b) for calcite resulting from open system CO_2 degassing (CO2-DIC), coupled CO_2 degassing and calcite precipitation (CO2-DIC-CC), and calcite precipitation from groundwater (DIC-CC). These are calculated for both the carbon and oxygen isotope system using a Rayleigh distillation approach similar to Kampman et al. (2012). For example, for the progressive formation of calcite from bicarbonate, the carbon isotope ratios can be calculated from Eq. (4):

$$\delta^{13}C = \delta^{13}C_o - [1000 \times ln\alpha_{product-HCO3}(1-F)] \quad \text{Eq. (4)}$$

where $\delta^{13}C_o$ is the starting carbon isotope ratio for HCO_3^- in solution, and F is the fraction of the C remaining in solution. Temperature dependent equilibrium fractionation factors (α) for carbon isotopes in the calcite, CO_2, dissolved inorganic carbon (DIC) system are derived from Deines et al. (1974). We assume that the paleofluids were slightly acidic (~6.5) and near the equivalence point of H_2CO_3 and HCO_3^- to compute the $\alpha_{DIC\text{-}CO2}$ (Gilfillan et al., 2009). This is consistent with pH and geochemical observations at Pah Tempe hot springs and Pumpkin spring (Crossey et al., 2009; Nelson et al., 2009). Assuming the precipitation of calcite based on: $CaCO_{3(calcite)} + CO_{2(g)} + H_2O \Leftrightarrow 2HCO_{3\,(aq)}^- + Ca^{2+}{}_{(aq)}$, the formation of calcite from HCO_3^- in solution partitions, on a molar basis, the carbon equally between calcite and CO_2. Using the approach of Kampman et al. (2012), the net fractionation factor between the products and the bicarbonate in solution based on Eq. (5) is:

$$\alpha_{product\text{-}HCO3} = 1/2\ (\alpha_{calcite\text{-}HCO3}) + 1/2(\alpha_{DIC\text{-}CO2}) \quad \text{Eq. (5)}$$

Similarly, the oxygen isotope fractionation factor is calculated using Eq. (6):

$$\alpha_{product\text{-}HCO3} = 1/3(\alpha_{CO2\text{-}HCO3}) + 1/2(\alpha_{calcite\text{-}HCO3}) + 1/6(\alpha_{H2O\text{-}HCO3}) \quad \text{Eq. (6)}$$

The oxygen isotope system temperature dependent fractionation factors are derived from published relationships (O'Neil et al., 1969; O'Neil et al., 1975; Beck et al., 2005).

Focusing on vein set 1 and a range of temperatures observed from fluid inclusion, the computed trends cannot explain the observed data (Fig. 4 b). Rayleigh fractionation trends under equilibrium conditions for CO_2 degassing and coupled CO_2 degassing + calcite precipitation <85 °C yield positive correlations that are *not* similar to the

Deleted: 3
Deleted: 3
Deleted: 5
Deleted: 5
Deleted: 6
Deleted: ¶
Deleted: 6
Deleted: 7
Deleted: 7
Deleted: 3
Formatted: Font: Italic

observed slope or range of values in set 1 calcite veins. Based on this analysis, it is unlikely that open system processes such as these are major phenomenon involved in the formation of calcite veins in the Hurricane fault zone. It is important to note that these Rayleigh fractionation models assume isotopic equilibrium. Rapid degassing and calcite precipitation may result in disequilibrium and kinetic fractionation that cannot be quantitatively addressed. However, we do not observe vapor-rich fluid inclusion in the calcite veins, which would be expected if CO_2 degassing was a major process.

To summarize these analyses and interpretations, most of the vein C and O isotopic compositions observed can be explained by a combination of the mixing of two primary fluid endmembers over a range of temperatures, with possible second order impacts from open system processes such as degassing during calcite precipitation. Vein set 1 is best explained by formation over a range of temperatures from the low-salinity endmember. Most of the values in set 2 and 3 can be explained by a mixture of the low-salinity meteoric and the sedimentary brine end members and precipitation over a range of temperatures. Vein set 4 requires addition of a much lower $\delta^{13}C$ component to the fluids responsible for vein set 3, likely derived from an organic source.

5.3 Implications of vein geochronology

Pilot U-Th geochronology on 5 samples indicates that calcite veins formed from 539 to 86 ka. These samples are from two different sample locations (1-2 and 1-4) separated by 13 km along strike (Fig. 2, 6), and from vein sets 1, 3, and 4. Specifically, at location 1-2, hosted in limestone, calcite vein growth occurred at 133 ka and 86 ka (set 4). Based on the interpreted growth direction of this vein, the dated laminations are chronologically consistent and suggest that the numerous vein laminations formed over a period of ~47 ka (Fig. 5 b). At location 1-4, hosted in sandstone, veins formed at 539 and 288 ka (set 1) and 86 ka (set 3). As described in the results, the dates are consistent with interpreted observed cross-cutting relationships, including the 86 ka calcite lamination cutting 288 ka calcite cemented brecciated sandstone (Fig. 6a).

Based on the stable isotope results and analyses, the 539 and 288 ka veins are likely associated with the low-salinity meteoric water endmember (Fig. S7) and formed at moderate temperatures (60-70 °C). The 113 ka and both 86 ka veins are best associated with ~100 °C saline groundwater, with varying contributions of a low $\delta^{13}C$ carbon source (Fig. S7). The 86 ka sample from location 1-2 has the lowest $\delta^{13}C$ (-7 ‰) observed in this study, and as discussed in section 5.2 requires an organic carbon source not observed at other locations.

Although this data set is small, it suggests punctuated vein forming events with some consistency along fault strike. Interestingly, these two fault locations appear to preserve the 86 ka fluid flow event, within analytical error, both requiring similar composition and temperature fluids, suggesting that the fluid circulation events have continuity over at least ~13 km of fault zone strike. More geochronological work is needed to evaluate if these crosscutting relationships are more broadly consistent along the fault zone. These dates can be used along with constraints on fault

Deleted: processes

Formatted: Subscript

Deleted:

Deleted: 5

Deleted: veins

Deleted: formed

Deleted: vein growth direction and

Deleted: 5

Deleted: 6

Deleted: 6

slip rate to estimate the maximum depth of vein formation. Using the published slip rate estimates of 0.44 to 0.57 mm/y (Lund et al., 2007), this equates to vein formation depths of ~40 to 300 m. However, this assumes negligible exhumation of the footwall over the last 540 ka, and are minimum estimates. Using the local incision rate of the Virgin River through the footwall of 338 m/Myr (Walk et al., 2019) as a maximum estimate of footwall exhumation, this suggests a maximum depth of vein formation of 70 to 480 m. Consistent with the findings at thermal springs along the Hurricane fault-zone (Crossey et al., 2006; Crossey et al., 2009; Nelson et al., 2009), this indicates that deeply-circulated thermal fluids are moving up the fault zone, advecting deeper geotherms towards the surface, and mixing with shallow meteoric fluids. The relatively shallow depth of these processes is notable, and has been observed at other major normal faults. For example, Smeraglia et al. (2018) documented Pleistocene synkinematic calcite mineralization along the Val Roveto fault (Apennines, Italy) that formed within the upper 350 m of the fault zone during mixing of deeply-derived fluids and meteoric infiltration.

Deleted: of
Deleted: T
Deleted:
Deleted: (2018).
Deleted: F

Although not the primary objective of this paper, the calcite vein textures in context of the preliminary geochronological results warrant a brief discussion. The vein wall breccias and laminated calcite veins observed along the Hurricane fault share similar characteristics to those in other major fault zones that have been attributed to co-seismic or post-seismic sealing (e.g., Nuriel et al., 2011; Nuriel et al., 2012; Smeraglia et al., 2018). These fracture openings filled with laminated growth bands of fibrous calcite crystal are indicative of post-fracture opening sealing (crack-seal cycle) (Ramsay, 1980). These suggest fluid-pressurization and fluid flow cycles associated with periodic fracturing in the fault damage zone, possibly due to seismic activity (e.g., Sibson, 1994). Williams et al. (2017b) showed that detailed U-Th dating of these types of laminated veins inform the periodic nature of fracture opening and sealing via calcite precipitation and argue these are associated with seismic events. Specifically, they documented 13 seismic events between 550 ka and 150 ka and use this to estimate long-term earthquake recurrence intervals. In addition to earthquakes, Pleistocene climatic cycles could influence groundwater flow and fluid pressure, and possibly be associated with vein forming events similar to what is observed at the Little Grand Wash and Salt Wash faults (e.g., Kampman et al., 2012). We have documented 4 such events in the last ~540 ka, suggesting that a similar high-resolution geochronological study could yield meaningful information about the long-term recurrence of fluid-flow triggering events along the Hurricane fault zone, whether triggered by seismicity or linked to climatic cycles.

Deleted: F

6 Summary and Conclusions

Integrated calcite vein stable isotope geochemistry, fluid inclusion microthermometry and U-Th geochronology document the nature of paleofluids circulating in the Hurricane fault over the last ~540 ky. Our results indicate that calcite veins form in the footwall damage zone of the fault from mixtures of two main fluids over a range of temperatures. These include a relatively low salinity meteoric-affinity groundwater and a salty sedimentary formation water. Carbon sources are more ambiguous, but likely include significant contributions from crustal or magmatic CO_2 and carbonate bedrock, along with lesser amounts from hydrocarbons. Fluid inclusion microthermometry temperatures from ~45 to 160 °C indicating that these fluids have circulated deeply (up to 6 km) prior to flowing up the Hurricane fault zone. Our pilot geochronology is sparse (5 dates) but supports punctuated vein forming events at 539, 288, 113,

Deleted: F
Deleted: 9

and 86 ka. Considering the published long-term slip rates along the Hurricane fault, these veins likely formed in the upper ~500 m of the crust. Present-day up flow of similar composition fluids occurs at Pah Tempe hot spring and where the fault cuts the Colorado River in Grand Canyon at Pumpkin and Travertine Grotto springs.

These results have implications for how the paleohydrology of the Hurricane fault changes spatially and through time. Calcite cemented fault breccia and laminated, fibrous calcite veins are suggestive of cycles of fracture opening and healing (i.e., crack-seal textures). Deep groundwater circulation and fault processes result in high pore pressures in the fault zone, and subsequent fracturing triggers up flow of CO_2-charged thermal fluids, fluid-rock interaction in the fault zone, and mixing with other ground waters. Calcite mineralization and veining from these flowing fluids heals breccias and fractures. The multiple generations of cross-cutting veins and laminated veins indicates that healed parts of the fault have experienced this cycle multiple times, and will have strongly effected the flow properties of the fault zone. Data from this study show that these linked mechanical and hydrological processes are occurring in the upper ~500 meters of the fault zone and is occurring periodically over ~180 km of fault strike. We conclude that the Hurricane fault imparts a strong influence on regional flow of crustal fluids, and that the formation of veins in the shallow parts of the fault damage zone has important implications for fault strength in the upper most part of the crust.

Deleted: F

Deleted: 40–300

Deleted: F

Deleted: 40 – 300 m

Deleted: F

7 Data Availability

Readers are invited to access the full data set archived on the EarthChem Library: https://doi.org/10.26022/IEDA/111542. (Newell and Koger, 2020).

8 Supplemental Information

Supplemental information, tables, figures are available at the following link: XXXXXX.

9 Author Contributions

Jace Koger conducted the field sample collection, sample preparation, and sample analyses as part of the requirement for his MSc in Geology from Utah State University (Koger, 2017). Dennis Newell was the thesis supervisor, provided assistance and mentorship on sampling and analytical techniques, guidance on data analysis, and is the corresponding author for the preparation of this manuscript.

10 Competing Interests

None.

11 Acknowledgements

We thank Andrew Lonero (USU Geosciences) and Diego Fernandez (University of Utah) for their assistance with stable isotopic and U-Th analyses, respectively. Funding for this research was provided by a Geological Society of America Student Research Grant to J. Koger and the Department of Geosciences at USU. This manuscript greatly benefitted from constructive reviews by Billy Andrews and Matthew Steele-MacInnis.

Tables and Figures

725

Table 1. Calculated paleofluid $\delta^{13}C$ and $\delta^{18}O$ from calcite C and O stable isotopes and microthermometry

Field Station	Sample ID	$\delta^{13}C_{cc}$ ‰ (VPDB)	$\delta^{18}O_{cc}$ ‰ (SMOW)	T_h (°C)	T_m (°C)	wt % NaCl[a]	$\delta^{13}C_{CO2}$[b] ‰ (VPDB)	$\delta^{18}O_{H2O}$[c] ‰ (SMOW)
1-2	JK15HR41	0.55	22.6	102.5 ± 25.0	-7.5 ± 1.7	11.0 ± 1.4	-4.3 ± 1.1	5.6 ± 2.7
1-4	JK15HR110	0.50	10.0	75.8 ± 2.3	-2.2 ± 0.9	3.7 ± 0.5	-5.7 ± 0.1	-10.0 ± 0.3
3-1	JK15HR151	1.27	9.8	66.7 ± 11.0	-0.8 ± 0.3	1.4 ± 0.6	-5.4 ± 0.7	-11.4 ± 1.5
3-4	JK15HR160	0.35	20.2	71.6 ± 9.8	-3.2 ± 1.2	5.2 ± 1.8	-6.1 ± 0.6	-0.5 ± 1.3
3-5	JK15HR169	0.77	18.3	72.2 ± 8.7	-2.0 ± 1.9	4.7 ± 2.6	-5.6 ± 0.5	-2.3 ± 1.2
5-2	JK15HR255	1.73	13.5	70.1 ± 7.0	-1.0 ± 0.2	1.7 ± 0.7	-4.8 ± 0.4	-7.2 ± 1.0
-	Pah Tempe HS[d]	-	-	-	-	0.8	-5.5	-13.0
-	Pumpkin Spr[e]	-	-	-	-	1.1	-6.1	-10.6
	Travertine Grotto[e]	-	-	-	-	0.2	-	-10.8

[a,b,c] calculated using Eq. (2), (4), and (3), respectively
[d]Nelson et al. (2004); [e]Crossey et al. (2009)

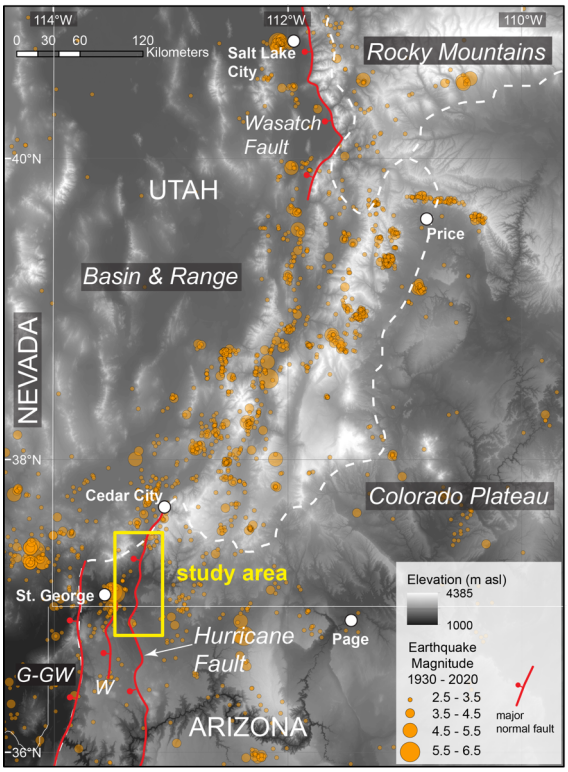

730 **Figure 1:** Location of the Hurricane fault and study area along the boundary between the Colorado Plateau and Basin and Range tectonic provinces in the western U.S. The fault is located within the Intermountain Seismic belt as delineated by the depicted >M 2.5 earthquakes recorded between 1930 – 2020 (USGS, 2020). Other notable faults in the region include the Gunlock-Grand Wash (G-GW) and Wasatch faults. (Digital Elevation, SRTM 1 Arc-Second Global 10.5066/F7PR7TFT, courtesy of the U.S. Geological Survey)

735

Deleted: F

Deleted: from

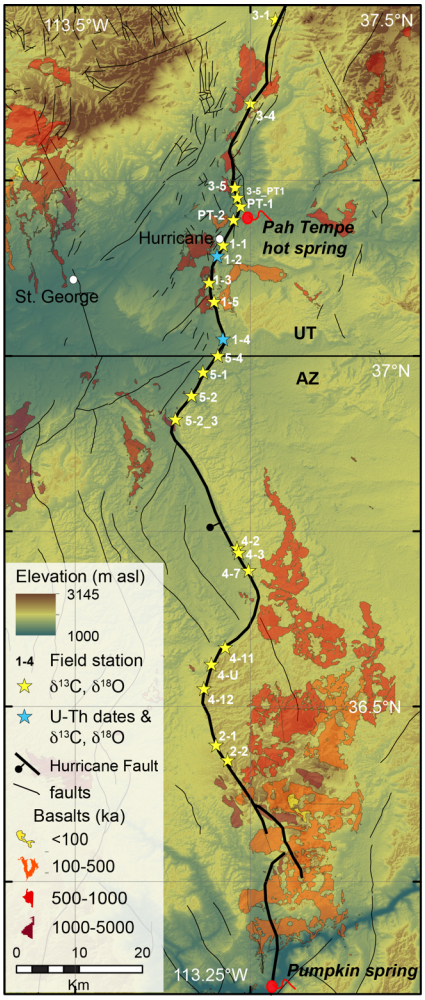

740 **Figure 2:** The Hurricane fault extent in southern Utah and northern Arizona with the 23 Field Stations investigated in this study. Note that C and O isotope values from calcite veins are reported for all field sites. Additionally, U-Th dates are reported from stations 1-2 and 1-4. Locations of Pah Tempe and Pumpkin springs are shown. Travertine Grotto is located south of map extent. Geology from (Billingsley and Workman, 2000; Billingsley and Wellmeyer, 2003; Rowley et al., 2008). (Digital Elevation, SRTM 1 Arc-Second Global 10.5066/F7PR7TFT, courtesy of the U.S. Geological Survey)

745

Deleted: F

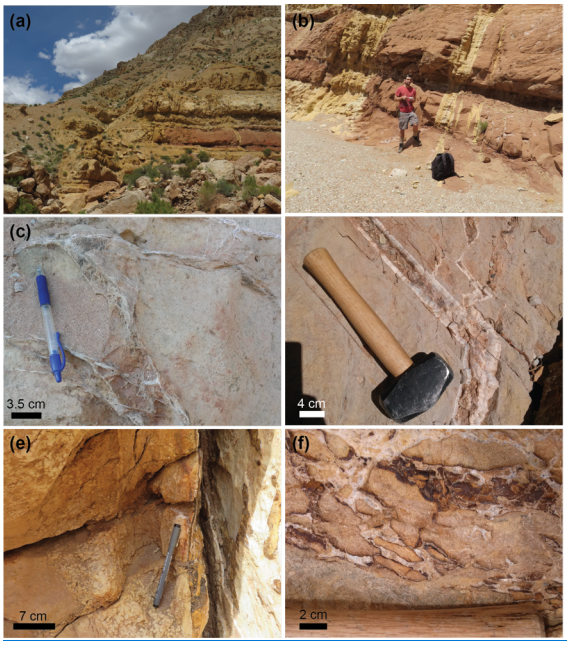

Figure 3. (a) Looking north along Hurricane fault trace with colluvium in the hanging wall offset against the Permian Queantoweap Sandstone. Note the bleaching along the fault trace and in horizontal strata of the Queantoweap Sandstone; **(b)** Decimeter to meter-scale bleached fractures cutting Queantoweap Sandstone, J. Koger for scale; **(c)** Boxwork sparry calcite veins; **(d)** Laminated, cm-scale calcite vein with minor intergrown hematite – cutting cherty limestone host rock; **(e)** Laminated calcite vein with minor hematite cutting Queantoweap Sandstone. Note the small calcite concretions cementing the sandstone parallel to the vein trace; **(f)** Calcite and hematite cemented breccia in sandstone host rock.

Formatted: Font: Bold
Formatted: Font: Bold
Formatted: Font: Bold
Formatted: Font: Bold
Formatted: Font: Bold

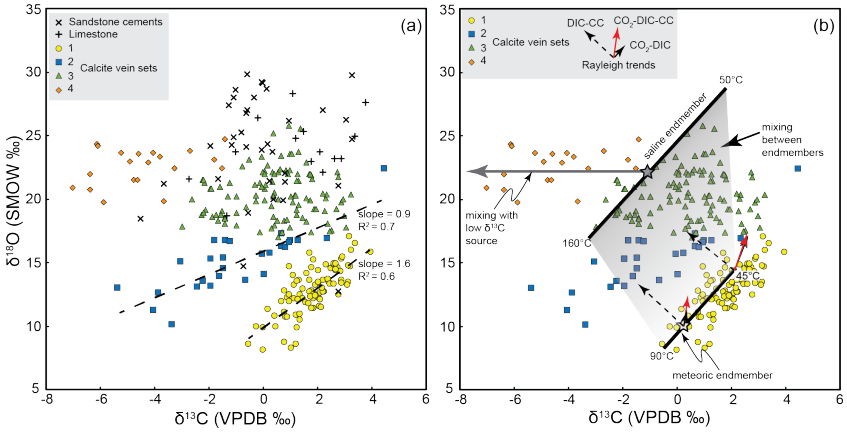

Figure 4 (a) Calcite oxygen and carbon stable isotope values for veins and host rocks along the Hurricane fault. Host rock values are from bulk limestone samples and from calcite cemented sandstones. The veins are divided into 4 veins sets for analysis. Note the trend line slopes for vein sets 1 and 2 **(b)** Paleofluid interpretations integrating the isotopic and fluid inclusion microthermometry results. Mixing scenarios depicted include the mixing of two endmember fluids over a range of temperature and the mixing with a low $\delta^{13}C$ CO_2 source. Also shown are the open-system Rayleigh fractionation trends due progressive precipitation of calcite from water dissolved inorganic carbon (DIC-CC), progressive CO_2 loss from the water dissolved inorganic carbon (CO2-DIC), and the combined effects of CO_2 degassing and calcite precipitation (CO2-DIC-CC).

Deleted: ¶

Deleted: 3

Deleted: F

Formatted: Subscript

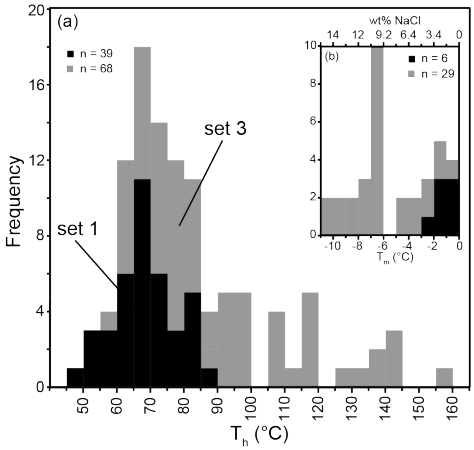

Figure 5: (a) Fluid inclusion (2-phase) homogenization temperatures from vein set 1 and 3. **(b)** Fluid inclusion melting temperatures from vein sets 1 and 3 and the calculated salinity as wt% NaCl (see text for details).

Deleted: 4

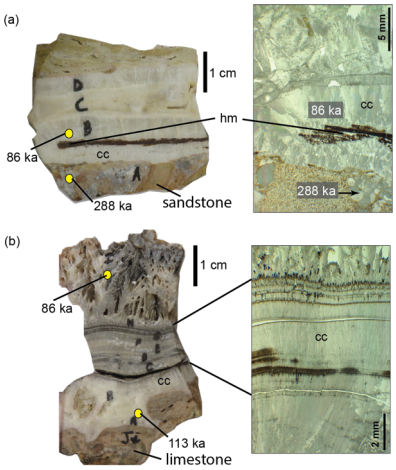

Figure 6: (a) Laminated calcite vein from location 1-4 and associated U-Th dates (samples JK15HR110 and JK15HR111). Hand specimen (left) and plane-polarized photomicrograph (right) shown. Note the calcite cemented brecciated sandstone forming the vein wall. The laminated calcite vein shows at least 4 episodes of calcite precipitation. The calcite cement in the wall breccia is 288 ka and the first lamination growing on the vein wall is 86 ka. **(b)** Laminated calcite vein from location 1-2 that is hosted in marine limestone. U-Th dates (JK15HR27 and JK15HR35) are shown on the hand specimen. The dates indicate growth outward from the limestone wall from 113 ka to 86 ka. Multiple dense laminations are visible in hand sample, and the plane polarized photomicrograph shows these are constructed of fibrous calcite crystals that terminate at discrete boundaries. The outermost (86 ka) layer is characterized by higher porosity vuggy calcite crystals suggestive of growth into free fluids.

Deleted: 5

Deleted: 9

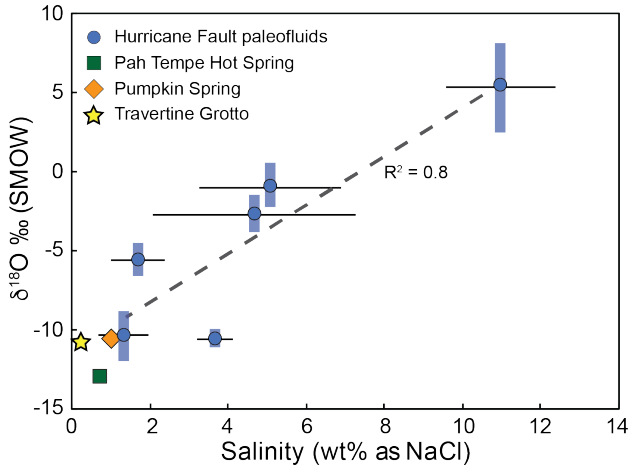

Figure 7. Calculated paleofluid oxygen isotope composition versus fluid salinity determined by fluid inclusion microthermometry. The strong positive correlation of $\delta^{18}O$ and salinity ($R^2 = 0.8$) is interpreted as a mixing trend between and low salinity, meteoric water and high salinity sedimentary brine endmember. For comparison, the composition of Pah Tempe, Pumpkin, and Travertine Grotto springs are included, are very similar in composition to the low salinity endmember.

Deleted: 6

Deleted: -affinity groundw

Deleted: ater

References

Anderson, R. E., and Mehnert, H. H.: Reinterpretation of the history of the Hurricane fault in Utah, in: Basin and Range Conference Guidebook: Geological Society of Nevada, Rocky Mountain Association of Geologists, and Utah Geological Society, edited by: Newman, G. W., 145-165, 1976.

Armstrong, R. L.: Sevier orogenic belt in Nevada and Utah, Geological Society of America Bulletin, 79, 429-458, 1968.

Axen, G. J., Taylor, W. J., and Bartley, J. M.: Space-time patterns and tectonic controls of Tertiary extension and magmatism in the Great Basin of the western United States, Geological Society of America Bulletin, 105, 56-76, 1993.

Baedecker, M. J., Cozzarelli, I. M., Eganhouse, R. P., Siegel, D. I., and Bennett, P. C.: Crude oil in a shallow sand and gravel aquifer—III. Biogeochemical reactions and mass balance modeling in anoxic groundwater, Applied Geochemistry, 8, 569-586, 1993.

Bahr, C. W.: Virgin oil field, Washington County, Utah, in: Guidbook to the geology of southwestern Utah: Transition between basin-range and Colorado plateau provinces, edited by: Heylmun, E. B., Intermountain Association of Petroleum Geologists, Salt Lake City, 169 - 171, 1963.

Bakker, R. J.: Package FLUIDS 1. Computer programs for analysis of fluid inclusion data and for modelling bulk fluid properties, Chemical Geology, 194, 3-23, 2003.

Ballentine, C. J., Burgess, R., and Marty, B.: Tracing Fluid Origin, Transport and Interaction in the Crust, in: Reviews in Mineralogy & Geochemistry - Noble Gases in Geochemistry and Cosmochemistry, edited by: Porcelli, D., Ballentine, C. J., and Wieler, R., Mineralogical Society of America, Washington D.C., 539-614, 2002.

Beck, W. C., Grossman, E. L., and Morse, J. W.: Experimental studies of oxygen isotope fractionation in the carbonic acid system at 15, 25, and 40 C, Geochimica et Cosmochimica Acta, 69, 3493-3503, 2005.

Benedicto, A., Plagnes, A., Vergely, P., Flotte, N., and Schultz, R. A.: Fault and fluid interaction in a rifted margin: integrated study of calcite-sealed fault-related structures (southern Corinth margin), in: The Internal Structure of Fault Zones: Implications for Mechanical and Fluid-Flow Properties, edited by: Wibberley, C. A. J., Kurz, W., Imber, J., Holdsworth, R. E., and Collettini, C., Geological Society of London, 257-275, 2008.

Bergman, S., Huntington, K. W., and Crider, J. G.: Tracing paleofluid sources using clumped isotope thermometry of diagenetic cements along the Moab Fault, Utah, American Journal of Science, 313, 490-515, 2013.

Best, M., and Brimhall, W.: Late Cenozoic alkalic basaltic magmas in the western Colorado Plateaus and the Basin and Range transition zone, USA, and their bearing on mantle dynamics, Geological Society of America Bulletin, 85, 1677-1690, 1974.

Biek, R.: Geologic Map of the Hurricane Quadrangle Washington County, Utah: Utah Geological Survey Map, 187, 2003.

Biek, R., Rowley, P., Hayden, J., Hacker, D., Willis, G., Hintze, L., Anderson, R., and Brown, K.: Geologic map of the St. George and east part of the Clover Mountains 30'X60' quadrangles, Washington and Iron counties, Utah, Utah Geological Society, 2010.

Billingsley, G., and Workman, J.: Geological map of the Littlefield 30' X 60' quadrangle, Mohave County, northwestern Arizona, U.S.G.S, 2000.

Billingsley, G., and Wellmeyer, J.: Geologic map of the Mount Trumbull 30' X 60' quadrangle, Mohave and Coconino Counties, northwestern Arizona, U.S.G.S., 2003.

Blakey, R.: Oil impregnated carbonate rocks of the Timpoweap Member Moenkopi Formation, Hurricane Cliffs area, Utah and Arizona, Utah Geology, 6, 45-54, 1979.

Bodnar, R., Lecumberri-Sanchez, P., Moncada, D., and Steele-MacInnis, M.: 13.5—Fluid inclusions in hydrothermal ore deposits, 2014.

Bodnar, R. J.: Revised equation and table for determining the freezing point depression of H2O-NaCl solutions, Geochimica et Cosmochimica Acta, 57, 683-684, 1993.

Boles, J. R., Eichhubl, P., Garven, G., and Chen, J.: Evolution of a hydrocarbon migration pathway along basin-bounding faults: Evidence from fault cement, AAPG bulletin, 88, 947-970, 2004.

Caine, J. S., Evans, J. P., and Forster, C. B.: Fault zone architecture and permeability structure, Geology, 24, 1025-1028, 1996.

Caine, J. S., and Minor, S. A.: Structural and geochemical characteristics of faulted sediments and inferences on the role of water in deformation, Rio Grande Rift, New Mexico, Geological Society of America Bulletin, 121, 1325-1340, 2009.

Caine, J. S., Bruhn, R. L., and Forster, C. B.: Internal structure, fault rocks, and inferences regarding deformation, fluid flow, and mineralization in the seismogenic Stillwater normal fault, Dixie Valley, Nevada, Journal of Structural Geology, 32, 1576-1589, 2010.

Cao, J., Jin, Z., Hu, W., Zhang, Y., Yao, S., Wang, X., Zhang, Y., and Tang, Y.: Improved understanding of petroleum migration history in the Hongche fault zone, northwestern Junggar Basin (northwest China): Constrained by vein-calcite fluid inclusions and trace elements, Marine and Petroleum Geology, 27, 61-68, 2010.

Chan, M. A., Parry, W., and Bowman, J.: Diagenetic hematite and manganese oxides and fault-related fluid flow in Jurassic sandstones, southeastern Utah, AAPG bulletin, 84, 1281-1310, 2000.

Chan, M. A., Parry, W. T., Petersen, E. U., and Hall, C. M.: 40Ar/39Ar age and chemistry of manganese mineralization in the Moab and Lisbon fault systems, southeastern Utah, Geology, 29, 331-334, 2001.

Chester, F. M., Evans, J. P., and Biegel, R. L.: Internal structure and weakening mechanisms of the San Andreas fault, Journal of Geophysical Research: Solid Earth, 98, 771-786, 1993.

Clayton, R. N., Friedman, I., Graf, D. L., Mayeda, T. K., Meents, W. F., and Shimp, N. F.: The origin of saline formation waters, I: Isotopic composition, Journal of Geophysical Research, 71, 3869-3882, 1966.

Crossey, L. J., Fischer, T. P., Patchett, P. J., Karlstrom, K. E., Hilton, D. R., Huntoon, P., Newell, D., and Reynolds, A.: Dissected hydrologic system at the Grand Canyon: Interaction between deeply derived fluids and plateau aquifer waters in modern springs and travertine, Geology, 34, 25-28, 2006.

Crossey, L. J., Karlstrom, K. E., Springer, A., Newell, D. L., Hilton, D. R., and Fischer, T. P.: Degassing of mantle-derived CO_2 and He from springs in the southern Colorado Plateau region - flux rates, neotectonic connections, and implications for groundwater systems, GSA Bulletin, 21, 1034 - 1053, 2009.

Crow, R., Karlstrom, K., Asmerom, Y., Schmandt, B., Polyak, V., and DuFrane, S. A.: Shrinking of the Colorado Plateau via lithospheric mantle erosion: Evidence from Nd and Sr isotopes and geochronology of Neogene basalts, Geology, 39, 27-30, 2011.

Deines, P., Langmuir, D., and Harmon, R. S.: Stable carbon isotope ratios and the existence of a gas phase in the evolution of carbonate ground waters, Geochimica et Cosmochimica Acta, 38, 1147-1164, 1974.

Dietrich, D., McKenzie, J. A., and Song, H.: Origin of calcite in syntectonic veins as determined from carbon-isotope ratios, Geology, 11, 547-551, 10.1130/0091-7613(1983)11<547:OOCISV>2.0.CO;2, 1983.

Dutson, S.: Effects of Hurricane Fault Architecture on Groundwater Flow in the Timpoweap Canyon of Southwestern, Utah [MS thesis]: Provo, Brigham Young University, 2005.

Edwards, R. L., Chen, J. H., and Wasserburg, G.: ^{238}U-^{234}U-^{230}Th-^{232}Th systematics and the precise measurement of time over the past 500,000 years, Earth and Planetary Science Letters, 81, 175-192, 1987.

Eichhubl, P., Davatzes, N. C., and Becker, S. P.: Structural and diagenetic control of fluid migration and cementation along the Moab fault, Utah, AAPG Bulletin, 93, 653-681, 2009.

Evans, J. P., Forster, C. B., and Goddard, J. V.: Permeability of fault-related rocks, and implications for hydraulic structure of fault zones, Journal of Structural Geology, 19, 1393-1404, 1997.

Fenton, C. R., Webb, R. H., Pearthree, P. A., Cerline, T. E., and Poreda, R. J.: Displacement rates on the Toroweap and Hurricane faults: Implications for Quaternary downcutting in the Grand Canyon, Arizona, Geology, 29, 1035 - 1038, 2001.

Fisher, J. R.: The volumetric properties of H_2O, J. Res. Us. Geol. Survey, 4, 189-193, 1976.

Forster, C. B., and Smith, L.: The influence of groundwater flow on thermal regimes in mountainous terrain: A model study, Journal of Geophysical Research, 94, 9439-9451, 1989.

Foxford, K., Walsh, J., Watterson, J., Garden, I. R., Guscott, S., and Burley, S.: Structure and content of the Moab Fault Zone, Utah, USA, and its implications for fault seal prediction, Geological Society, London, Special Publications, 147, 87-103, 1998.

Frery, E., Gratier, J.-P., Ellouz-Zimmerman, N., Loiselet, C., Braun, J., Deschamps, P., Blamart, D., Hamelin, B., and Sennen, R.: Evolution of fault permeability during episodic fluid circulation: Evidence for the effects fo fluid-rock interactions from travertine studies (Utah-USA), Tectonophysics, 651-652, 121-137, 2015.

Ghisetti, F., Kirschner, D., Vezzani, L., and Agosta, F.: Stable isotope evidence for contrasting paleofluid circulation in thrust faults and normal faults of the central Apennines, Italy, Journal of Geophysical Research: Solid Earth, 106, 8811-8825, 2001.

Gilfillan, S. M. V., Sherwood Lollar, B., Holland, G., Blagburn, D., Stevens, S., Schoell, M., Cassidy, M., Ding, Z., Zhou, Z., Lacrampe-Couloume, G., and Ballentine, C. J.: Solubility trapping in formation water as dominant CO_2 sink in natural gas fields, Nature, 458, 614-617, 2009.

Goldstein, R. H., and Reynolds, T. J.: Systematics of fluid inclusions in diagenetic minerals/ SEPM Short Course 31, Tulsa, OK, 199 pp., 1994.

Goldstein, R. H.: Fluid inclusions in sedimentary and diagenetic systems, Lithos, 55, 159-193, 2001.

Heller, P., Bowdler, S., Chambers, H., Coogan, J., Hagen, E., Shuster, M., Winslow, N., and Lawton, T.: Time of initial thrusting in the Sevier orogenic belt, Idaho-Wyoming and Utah, Geology, 14, 388-391, 1986.

Hendy, C. H.: The isotopic geochemistry of speleothems—I. The calculation of the effects of different modes of formation on the isotopic composition of speleothems and their applicability as palaeoclimatic indicators, Geochimica et cosmochimica Acta, 35, 801-824, 1971.

Heynekamp, M. R., Goodwin, L. B., Mozley, P. S., and Haneberg, W. C.: Controls on fault-zone architecture in poorly lithified sediments, Rio Grande Rift, New Mexico: Implications for fault-zone permeability and fluid flow, Washington DC American Geophysical Union Geophysical Monograph Series, 113, 27-49, 1999.

Hodson, K. R., Crider, J. G., and Huntington, K. W.: Temperature and composition of carbonate cements record early structural control on cementation in a nascent deformation band fault zone: Moab Fault, Utah, USA, Tectonophysics, 690, 240-252, 2016.

Hoefs, J.: Stable Isotope Geochemistry, 3 ed., Springer-Verlag, New York, 241 pp., 1987.

Humphreys, E., Hessler, E., Dueker, K., Farmer, G. L., Erslev, E., and Atwater, T.: How Laramide-age hydration of North American lithosphere by the Farallon Slab controlled subsequent activity in the Western United States, International Geology Review, 45, 575-595, 2003.

Kampman, N., Burnside, N. M., Shipton, Z. K., Chapman, H. J., Nicholl, J. A., Ellam, R. M., and Bickle, M. J.: Pulses of carbon dioxide emissions from intracrustal faults following climatic warming, Nature Geoscience, 5, 352-358, 2012.

Kim, S.-T., Coplen, T. B., and Horita, J.: Normalization of stable isotope data for carbonate minerals: Implementation of IUPAC guidelines, Geochimica et Cosmochimica Acta, 158, 276 - 289, 2015.

Knipe, R.: Faulting processes and fault seal, in: Structural and tectonic modelling and its application to petroleum geology, Elsevier, 325-342, 1992.

Koger, J. M.: Spatio-Temporal History of Fluid-Rock Interaction in the Hurricane Fault Zone, MS, Utah State University, 158 pp., 2017.

Krüger, Y., Stoller, P., Rička, J., and Frenz, M.: Femtosecond lasers in fluid-inclusion analysis: overcoming metastable phase states, European Journal of mineralogy, 19, 693-706, 2007.

Laubach, S. E., Eichhubl, P., Hilgers, C., and Lander, R.: Structural diagenesis, Journal of Structural Geology, 32, 1866-1872, 2010.

Laubach, S. E., Lander, R., Criscenti, L. J., Anovitz, L. M., Urai, J., Pollyea, R., Hooker, J. N., Narr, W., Evans, M. A., and Kerisit, S. N.: The role of chemistry in fracture pattern development and opportunities to advance interpretations of geological materials, Reviews of Geophysics, 57, 1065-1111, 2019.

Livaccari, R. F.: Role of crustal thickening and extensional collapse in the tectonic evolution of the Sevier-Laramide orogeny, western United States, Geology, 19, 1104-1107, 1991.

Lund, W., Hozik, M., and Hatfield, S.: Paleoseismic investigation and long-term slip history of the Hurricane Fault in southwestern UtahSpecial Study 119, Utah Geological Society, 81, 2007.

Marty, B., and Jambon, A.: C/^{3}He in volatile fluxes from the solid Earth: Implications for carbon geodynamics, Earth and Planetary Science Letters, 70, 196-206, 1987.

McCrea, J. M.: On the isotope chemistry of carbonates and a paleotemperature scale, The Journal of Chemical Physics, 18, 849-857, 1950.

Mozafari, M., Swennen, R., Balsamo, F., Clemenzi, L., Storti, F., El Desouky, H., Vanhaecke, F., Tueckmantel, C., Solum, J., and Taberner, C.: Paleofluid Evolution In Fault-Damage Zones: Evidence From Fault–Fold Interaction Events In the Jabal Qusaybah Anticline (Adam Foothills, North Oman), Journal of Sedimentary Research, 85, 1525-1551, 2015.

Mozley, P. S., and Goodwin, L. B.: Patterns of cementation along a Cenozoic normal fault:A record of paleoflow orientations, Geology, 23, 539-542, 1995.

Nelson, S. T., and Tingey, D. G.: Time-transgressive and extension-related basaltic volcanism in southwest Utah and vicinity, Geological Society of America Bulletin, 109, 1249-1265, 1997.

Nelson, S. T., Mayo, A. L., Gilfillan, S., Dutson, S. J., Harris, R. A., Shipton, Z. K., and Tingey, D. G.: Enhanced fracture permeability and accompanying fluid flow in the footwall of a normal fault: The Hurricane fault at Pah Tempe hot springs, Washington County, Utah, Geological Society of America Bulletin, 109, 1249-1265, 2009.

Newell, D. L., Jessup, M. J., Cottle, J. M., Hilton, D., Sharp, Z., and Fischer, T.: Aqueous and isotope geochemistry of mineral springs along the southern margin of the Tibetan plateau: Implications for fluid sources and regional degassing of CO_2, Geochemistry, Geophysics, and Geosystems, 9, Q08014, doi:08010.01029/02008GC002021, 2008.

Newell, D. L., Jessup, M. J., Hilton, D. R., Shaw, C. A., and Hughes, C. A.: Mantle-derived helium in hot springs of the Cordillera Blanca, Peru: Implications for mantle-to-crust fluid transfer in a flat-slab subduction setting, Chemical Geology, 417, 200 - 209, 2015.

Newell, D. L., and Koger, J. M.: Calcite vein C and O stable isotope values, fluid inclusion microthermometry, and U-Th dates from the Hurricane Fault zone, Utah and Arizona, USA., Interdisciplinary Earth Data Alliance (IEDA), 2020.

Nuriel, P., Rosenbaum, G., Uysal, T. I., Zhoa, J. X., Golding, S. D., Weinberger, R., Karabacak, V., and Avni, Y.: Formation of fault-related calcite precipitates and their implications for dating fault activity in the East Anatolian and Dead Sea fault zones, Geological Society, London, Special Publications, 359, 229-248, 2011.

Nuriel, P., Weinberger, R., Rosenbaum, G., Golding, S. D., Zhao, J., Tonguc Uysal, I., Bar-Matthews, M., and Gross, M. R.: Timing and mechanism of late-Pleistocene calcite vein formation across the Dead Sea Fault Zone, northern Israel, Journal of Structural Geology, 36, 43-54, 2012.

O'Neil, J. R., Adami, L. H., and Epstein, S.: Revised value for the ^{18}O fractionation between CO_2 and H_2O at 25°C, J. Res. US Geol. Surv, 3, 623-624, 1975.

O'Neil, R. R., Clayton, R. N., and Mayeda, T. K.: Oxygen isotope fractionation in divalent metal carbonates, Journal of Chemical Physics, 51, 5547-5558, 1969.

Pearthree, P. A., Menges, C. M., and Mayer, L.: Distribution, recurrence, and possible tectonic implications of late Quaternary faulting in ArizonaArizona Geological Survey OFR-83-20, 1983.

Quigley, M. C., Karlstrom, K., and Kelley, S.: Influence of Proterozoic and Laramide structures on the Miocene extensional strain field, SE Nevada, Geological Society of America Abstracts with Programs, 2002, 9,

Quirk, B. J., Mackey, G. N., Fernandez, D. P., Armstrong, A., and Moore, J. R.: Speleothem and glacier records of Late Pleistocene-Early Holocene climate change in the Western North American Interior, Journal of Quaternary Science, 35, 776-790, 2020.

Ramsay, J. G.: The crack-seal mechanism of rock deformation, Nature, 284, 135-139, 1980.

Rowley, P., Williams, V., Vice, G., Maxwell, D., Hacker, D., Snee, L., and Mackin, J.: Interim geologic map of the Cedar City 30' x 60' quadrangle, Iron and Washington Counties, Utah, Utah Geological Society, 2008.

Salomon, E., Rotevatn, A., Kristensen, T. B., Grundvåg, S. A., Henstra, G. A., Meckler, A. N., Gerdes, A., and Albert, R.: Fault-controlled fluid circulation and diagenesis along basin bounding fault systems in rifts – insights from the East Greenland rift system, Solid Earth Discuss., 2020, 1-37, 10.5194/se-2020-72, 2020.

Sharp, Z. D.: Principles of Stable Isotope Geochemistry, Pearson/Prentice Hall, Upper Saddle River, N.J., 344 pp., 2007.

Sherwood Lollar, B., Ballentine, C. J., and O'Nions, R. K.: The fate of mantle-derived carbon in a continental sedimentary basin: Integration of C/He relationships and stable isotope signatures, Geochimica et Cosmochimica Acta, 61, 2295-2307, 1997.

Shipton, Z. K., Evans, J. P., Kirschner, D., Kolesar, P. T., Williams, A. P., and Heath, J.: Analysis of CO2 leakage through 'low-permeability'faults from natural reservoirs in the Colorado Plateau, east-central Utah, Geological Society, London, Special Publications, 233, 43-58, 2004.

Sibson, R. H.: Crustal stress, faulting and fluid flow, Geological Society, London, Special Publications, 78, 69-84, 1994.

Sibson, R. H.: Structural permeability of fluid-driven fault-fracture meshes, Journal of Structural Geology, 18, 1031-1042, 1996.

Sibson, R. H.: Fluid involvement in normal faulting, Journal of Geodynamics, 29, 469-499, 2000.

Smeraglia, L., Bernasconi, S. M., Berra, F., Billi, A., Boschi, C., Caracausi, A., Carminati, E., Castorina, F., Doglioni, C., and Italiano, F.: Crustal-scale fluid circulation and co-seismic shallow comb-veining along the longest normal fault of the central Apennines, Italy, Earth and Planetary Science Letters, 498, 152-168, 2018.

Smith, R. B., Nagy, W. C., Julander, K., Viveiros, J. J., Barker, C. A., and Gants, D. G.: Geophysical and tectonic framework of the eastern Basin and Range-Colorado Plateau-Rocky Mountain transition, in: Geophysical Framework of the Continental United States, Geol. Soc. Am. Mem Boulder, CO, 205-233, 1989.

Sommer, S. N., and Budding, K. E.: Low-temperature thermal waters in the Santa Clara and Virgin River valleys, Washington County, Utah, in: Cenozoic Geology and Geothermal Systems of Southwestern Utah, edited by: Blackett, R. E., and Moore, J., Utah Geological Association, Salt Lake City, 81-95, 1994.

Stenner, H. D., and Pearthree, P. A.: Paleoseismology of the southern Anderson Junction section of the Hurricane Fault, northwestern Arizona and southwestern Utah, Arizona Geological Survery, Tucson, AZArizona Geological Survey Open-File Report 99-8, 1999.

Stewart, M. E., and Taylor, W. J.: Structural analysis and fault segment boundary identification along the Hurricane fault in southwestern Utah, Journal of Structural Geology, 18, 1017-1029, 1996.

Swanson, E. M., Wernicke, B. P., Eiler, J. M., and Losh, S.: Temperatures and fluids on faults based on carbonate clumped–isotope thermometry, American Journal of Science, 312, 1-21, 2012.

Tuccillo, M. E., Cozzarelli, I. M., and Herman, J. S.: Iron reduction in the sediments of a hydrocarbon-contaminated aquifer, Applied Geochemistry, 14, 655-667, 1999.

USGS: ANSS Comprehensive Earthquake Catalog, accessed April 20, 2020 athttps://earthquake.usgs.gov/earthquakes/search/, 2020.

Walk, C. J., Karlstrom, K. E., Crow, R. S., and Heizler, M. T.: Birth and evolution of the Virgin River fluvial system:~ 1 km of post–5 Ma uplift of the western Colorado Plateau, Geosphere, 15, 759-782, 2019.

Watkins, H., Bond, C. E., Healy, D., and Butler, R. W.: Appraisal of fracture sampling methods and a new workflow to characterise heterogeneous fracture networks at outcrop, Journal of Structural Geology, 72, 67-82, 2015.

Williams, R. T., Goodwin, L. B., Mozley, P. S., Beard, B. L., and Johnson, C. M.: Tectonic controls on fault zone flow pathways in the Rio Grande rift, New Mexico, USA, Geology, 43, 723-726, 2015.

Williams, R. T., Goodwin, L. B., and Mozley, P. S.: Diagenetic controls on the evolution of fault-zone architecture and permeability structure: Implications for episoldicity of fault-zone fluid transport in extensional basins, Geological Society of America Bulletin, 129, 464-478, 2017a.

Williams, R. T., Goodwin, L. B., Sharp, W. D., and Mozley, P. S.: Reading a 400,000-year record of earthquake frequency for an intraplate fault, Proceedings of the National Academy of Sciences, 114, 4893-4898, 2017b.

Williams, R. T., Beard, B. L., Goodwin, L. B., Sharp, W. D., Johnson, C. M., and Mozley, P. S.: Radiogenic isotopes record a 'drop in a bucket'–A fingerprint of multi-kilometer-scale fluid pathways inferred to drive fault-valve behavior, Journal of Structural Geology, 125, 262-269, 2019.

Yardley, B., Banks, D., Barnicoat, A., and Porter, T.: The chemistry of crustal brines: tracking their origins, in: Hydrothermal iron oxide copper-gold and related deposits: A global perspective, edited by: Porter, T., Porter Geological Publishing, Adelaide, 61-70, 2000.

Yonkee, W. A., and Weil, A. B.: Tectonic evolution of the Sevier and Laramide belts within the North American Cordillera orogenic system, Earth-Science Reviews, 150, 531-593, 2015.

Zandt, G., Myers, S. C., and Wallace, T. C.: Crust and mantle structure across the Basin and Range-Colorado Plateau boundary at 37°N latitude and implications for Cenozoic extensional mechanism, Journal of Geophysical Research: Solid Earth, 100, 10529-10548, 1995.

The following supplemental figures, tables, and descriptions support the main manuscript content.

S1. Supplemental geographic and stratigraphic information

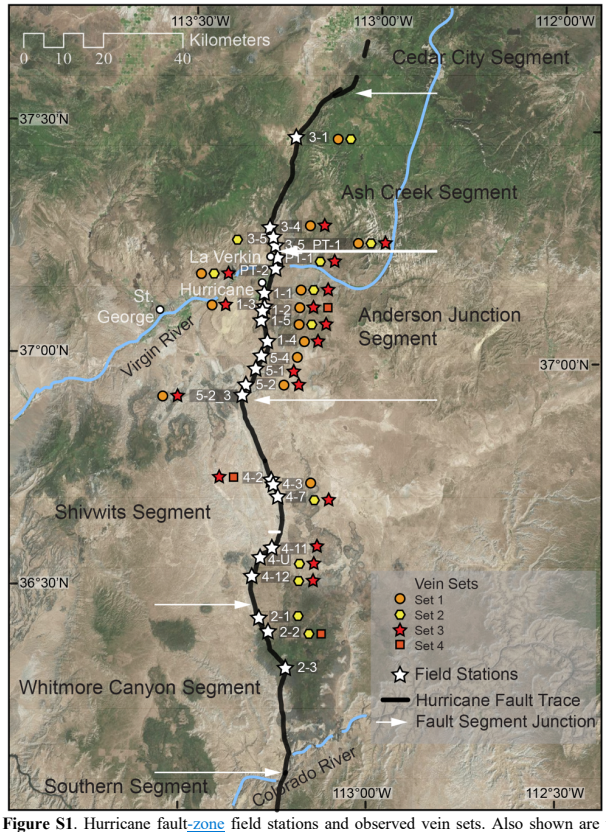

Figure S1. Hurricane fault-zone field stations and observed vein sets. Also shown are the Hurricane fault segment boundaries. (Image Source: Esri, DigitalGlobe, GeoEye, Earthstar Geographics, CNES/Airbus DS, USDA, USGS, AeroGRID, IGN, and the GIS User Community).

Deleted: F

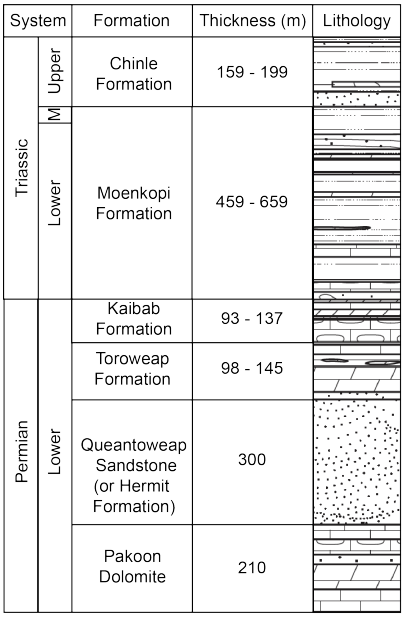

Figure S2. Representative stratigraphic column of units exposed in the study area along the trace of the Hurricane fault. Modified from (Biek, 2003; Dutson, 2005; Biek et al., 2010).

S2 Hurricane fault-zone fractures, veins, and alteration

S2.1 Fracture and vein orientations

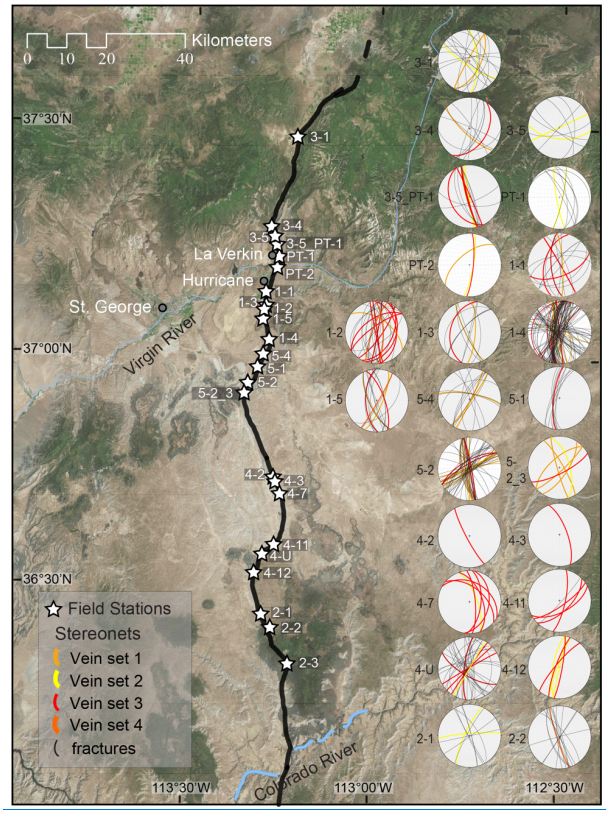

Figure S3. Fracture and vein orientation along the Hurricane fault-zone. Stereonets correspond to each field station and depict the veins sets and fractures measured in the footwall damage zone (stereonets include a total of 477 vein and fracture measurements).

S2.2 Calcite veins and fracture fills

Various morphologies of veins and fracture coatings are present along the main fault trace and in the footwall damage zone (Fig. S4). Cross-cutting veins at multiple sites indicate that multiple episodes of fracturing and mineralization occurred (Fig. S4 a). Calcite is ubiquitous as a fracture and vein mineral along the Hurricane fault zone. The majority (~70%) of veins observed are composed of sparry calcite, and are particularly common cutting limestone strata (Fig. S4 b). Interconnected, web-like "boxwork" calcite veins are common in sandstone within ~ 50 m of the main fault trace (Fig. S4 c). Other

Formatted: Font: 9 pt, Bold, English (UK)
Formatted: Normal
Formatted: Font: 9 pt
Deleted: 1
Deleted: commonly observed features nearby
Deleted: 3
Deleted: 3
Deleted: 3
Deleted: 3

precipitates include manganese oxides, hematite, and gypsum. Intergrown oxide and calcite veins are commonly observed in calcareous sandstone units that contain minor oxide cement (Fig. S4 d, e). The Permian Queantoweap Sandstone and Hermit Formation (stratigraphically correlative units) host many of these secondary minerals (e.g., sites 1-4 and 5-2 to 5-3). For example, manganese oxides are observed forming dendrites, associated with calcite veins in sandstone (Fig. S4 e). Although the majority of calcite plus oxide veins are found within sandstone strata, one location (site 1-2) hosts intergrown laminated calcite and minor hematite veins in cherty limestone of the Brady Canyon member of the Toroweap Formation (Fig. S4 f). These veins are located within a ~10-m-wide zone of intense fracturing (~5 m^{-1}). Bands of sparry to fibrous calcite crystals terminate into narrow bands of iron oxide (Fig. 5 b). Gypsum veins are also present and often associated with or stratigraphically near gypsum-rich strata (e.g., site 4-11).

S2.3 Breccia and slip surfaces

Mesoscopic structures associated with fault slip, rock fracture, and alteration along the Hurricane fault include but are not limited to fault-core breccias, brecciated veins, and striated slip surfaces (Fig. S5). Fault-core breccias along the main trace of the fault are well-exposed in two locations (sites 1-2 and 4-2) between the footwall damage zone and the buried trace of the fault, both hosted in cherty limestone units. These fault-core breccias exhibit grain size reduction of chert clast, and alternating bands of calcite and brecciated host rock (Fig S5 a). Brecciated veins are observed in fine-grained sandstones of the Queantoweap Sandstone and Hermit Formation, particularly at sites 1-4 and 5-2 to 5-3. They are cemented by calcite and minor hematite (Fig. S5 b). Angular clasts are jigsaw-piece shaped and heterogeneous in size, and there is evidence for multiple generations of brecciation and cementation. Cemented breccias are present within zones of relatively high fracture intensity (≥5 m^{-1}) and often associated with redox alteration (e.g., "bleaching") of the host rock (Fig. S5 c). Striated slip surfaces are common near the main fault trace in the damage zone at numerous study location, particularly those that comprise sandstone host rocks. They are commonly coated by slickenfibres of calcite that vary from <1 mm to multiple cm thick or intergrown calcite and hematite ≤2 mm thick (Fig. S5 d). Polished slip surfaces are composed of multiple discrete planes, implying multiple stages of slip. Slickenlines have a downdip orientation indicating primarily dip-slip movement.

Deleted: 3
Deleted: Hermit
Deleted: Formation
Deleted: s
Deleted: 3
Deleted: 3
Deleted: dense
Deleted: 2
Deleted: F
Deleted: 4
Deleted: 4
Deleted: 4
Deleted: density
Deleted: 4
Deleted: 4

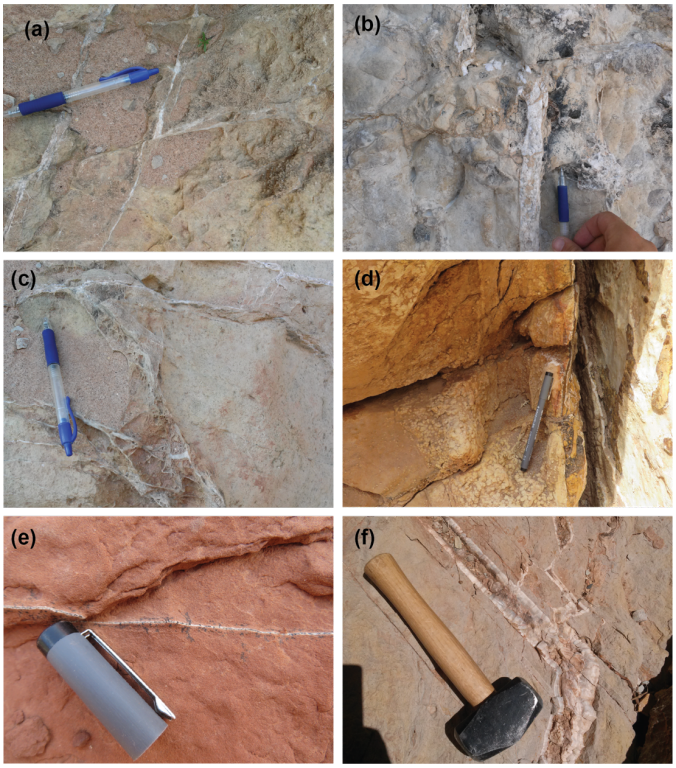

Figure S4. (a) Sets of sparry calcite veins showing offset; (b) Sparry calcite vein in limestone host rock; (c) Boxwork calcite veins; (d) Laminated calcite vein with minor hematite cutting sandstone. Note the small calcite concretions cementing the sandstone parallel to the vein trace; (e) Manganese oxide dendrites associated with mm-scale calcite vein in sandstone; (f) Laminated, cm-scale calcite vein with minor intergrown hematite – cutting cherty limestone host rock.

Deleted: 3

Formatted: Font: Not Bold

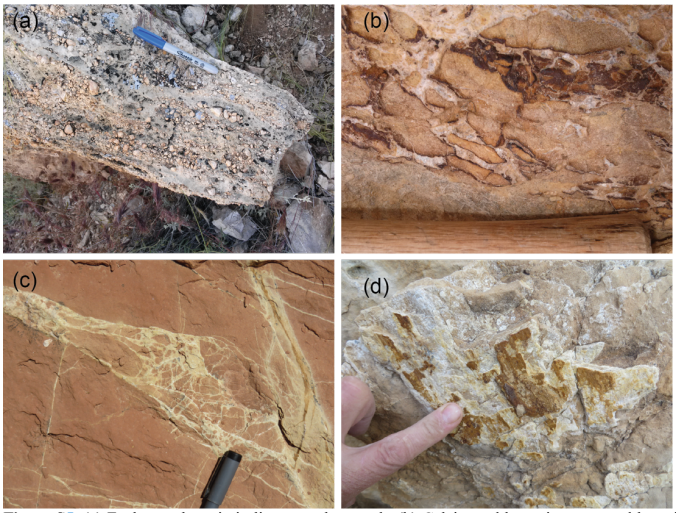

Figure S5. (a) Fault-core breccia in limestone host rock; (b) Calcite and hematite cemented breccia in sandstone host rock (part of rock hammer handle for scale); (c) Brecciated red (hematite cemented) sandstone showing bleaching and minor calcite veining along fractures; (d) Striated fault surfaced with calcite and hematite mineralization

S2.4 Host rock alteration

Where the siliciclastic strata of the Permian Queantoweap Sandstone (or Hermit Formation) are present in the footwall damage zone, evidence for fluid-rock interaction includes fracture-related redox features and intragranular cements. Fracture-parallel bands of white to light tan alteration (commonly referred to as bleaching) are found along fault-parallel fractures (Fig. S6 a, b). Bleaching indicates mobilization iron oxide cements in these sandstones. Bleaching halos vary in width with some on the order of 0.1 to 3 cm (Fig. S6 c) and others on the decimeter to meter-scale (Fig. S6 a, b). Alternating stratigraphic horizons are also bleached separated by unaltered strata (Fig. S6 a, c). The degree of sandstone cementation by calcite also changes in the fault zone. Near the fault trace, calcite cementation, including the presence of calcite concretions is greatest adjacent to fractures, and fractures hosting calcite veins (Fig. S6 d).

Deleted: 4
Formatted: Font: Not Bold
Deleted: 3
Deleted: and
Deleted: 5
Deleted: 5
Deleted: 5
Deleted: 5
Deleted: 3

Figure S6. (a) Looking north along Hurricane fault trace. Note the offset Permian Queantoweap Sandstone displaying bleaching along the fault trace and in horizontal strata; (b) Decimeter to meter-scale bleached fractures cutting Queantoweap Sandstone; (c) Densely fractured silty sandstone in the Hermit Formation showing mm- to cm-scale bleaching along fractures; (d) Bedding parallel bleaching in siltstones bounded by unbleached strata.

Deleted: 5

Formatted: Font: Not Bold

Deleted: F

Deleted: Hermit Formation

S3 Data table and figure supplements

Table S1. Location of 23 Field Stations along the Hurricane Fault

Field Station	Latitude[a]	Longitude
3-1	37.477510	-113.21409
3-4	37.361312	-113.25263
3-5	37.237774	-113.27133
3-5_PT1	37.227990	-113.25961
PT-1	37.212103	-113.26174
PT-2	37.191258	-113.27319
1-1	37.157048	-113.28758
1-2	37.137324	-113.29661
1-3	37.103990	-113.30294
1-5	37.080825	-113.30608
1-4	37.017787	-113.28893
5-4	36.996654	-113.30263
5-1	36.973909	-113.31452
5-2	36.942954	-113.33335
5-2_3	36.925742	-113.35111
4-2	36.725976	-113.26352
4-3	36.714396	-113.25492
4-7	36.695012	-113.24731
4-11	36.580715	-113.28505
4-U	36.569903	-113.29930
4-12	36.519993	-113.31926
2-1	36.443720	-113.29808
2-2	36.421994	-113.28260

[a] WGS 84 datum

Table S2. U-Th data for the 5 calcite veins. All ratios are activity ratios.

Sample ID	$^{230}Th/^{238}U_{true}$ [a]	$^{234}U/^{238}U_{true}$	$^{230}Th/^{232}Th_{true}$	$^{232}Th/^{238}U_{true}$	$\delta^{235}U$ rel to CRM145	$\delta^{235}U$ stds rel to CRM145	age (y)[b]	$^{234}U/^{238}U_{init}$
JK15HR110	0.9373	1.007	1510	6.21E-04	0.0		287,856 ± 5757	
JK15HR111	0.8306 ± 0.0008	1.469 ± 0.002	588±1.23	1.41E-03 ± 2.85E-06	-0.3±0.2	-0.3±0.3	85,993 ± 196	1.598 ± 0.004
JK15HR103	1.1609	1.120	87	1.33E-02	-0.1		539,304 ± 10786	
JK15HR27	0.9437 ± 0.0009	1.403 ± 0.002	240±0.503	3.94E-03 ± 7.95E-06	0.5±0.	0.0±0.3	113,062 ± 315	1.555 ± 0.004
JK15HR35	0.8110	1.435	422	1.92E-03	0.0		86,233± 1725	

[a] Where reported, errors are 1-sigma. Due to slight method differences, these errors are not available for all samples
[b] Errors for JK15HR110 and 103 are estimated as 2%, rather than 1-sigma due to method differences

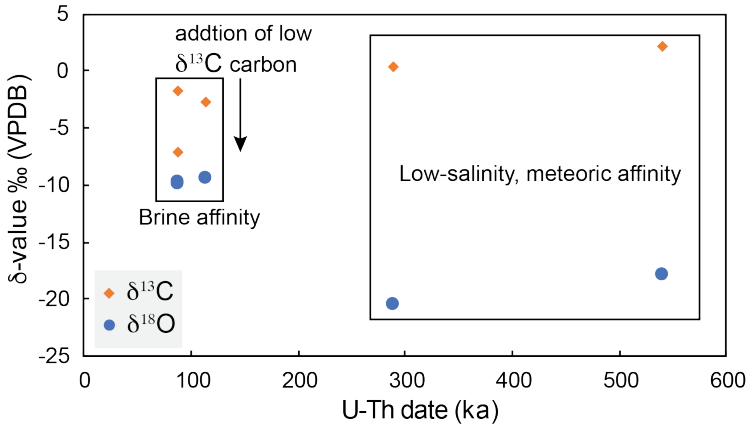

Figure S7. Carbon and oxygen stable isotope values and corresponding U-Th dates for the 5 dated samples. The likely fluid-endmember is identified based on stable isotope values.

Deleted: 6

References Cited

Biek, R.: Geologic Map of the Hurricane Quadrangle Washington County, Utah: Utah Geological Survey Map, 187, 2003.

Biek, R., Rowley, P., Hayden, J., Hacker, D., Willis, G., Hintze, L., Anderson, R., and Brown, K.: Geologic map of the St. George and east part of the Clover Mountains 30'X60' quadrangles, Washington and Iron counties, Utah, Utah Geological Society, 2010.

Dutson, S.: Effects of Hurricane Fault Architecture on Groundwater Flow in the Timpoweap Canyon of Southwestern, Utah [MS thesis]: Provo, Brigham Young University, 2005.